2005

Robust Initial Matching Of Free-form Objects Represented By Point Cloud Data

Nimun A. Jahangir

ROBUST INITIAL MATCHING OF FREE-FORM OBJECTS REPRESENTED BY POINT CLOUD DATA

(Spine title: Robust Initial Matching)

(Thesis format: Monograph)

by

Nimun A. Jahangir

Graduate Program in Engineering Science
Department of Mechanical and Materials Engineering

Submitted in partial fulfilment
of the requirements for the degree of
Master of Engineering Science

Faculty of Graduate Studies
The University of Western Ontario
London, Ontario, Canada
August, 2005

THE UNIVERSITY OF WESTERN ONTARIO

FACULTY OF GRADUATE STUDIES

CERTIFICATE OF EXAMINATION

Advisor	Examining Board
Dr. H. Y. Feng	Dr. S. F. Asokanthan
_____	_____
	Dr. A.V. Singh
Advisory Committee	_____
Dr. R. O. Buchal	Dr. Ken McIsaac
_____	_____
_____	_____

The Thesis by

Nimun A. Jahangir

entitled

Robust Initial Matching of Free-Form Objects

Represented by Point Cloud Data

is accepted in partial fulfillment of the

requirements for the degree of

Masters of Engineering Science

August 19, 2005
Date

Dr. M. D. Naish
Chairman of Examining Board

Abstract

Object matching of free-form surfaces is a key issue in the Computer-Aided Inspection because it aligns the design model and the manufactured product in the same coordinate system for a reliable conformance checking of the physical part to the specifications defined at the design stage. Presented in this thesis is a novel approach for robust initial matching of free-form objects represented by point cloud data while no prior information on correspondence or initial transformation is available. Delaunay pole sphere, obtained from the computational geometric technique Delaunay triangulation, has been employed as the specific property for searching correspondence instead of any intrinsic differential properties of the shape because no estimation method used to estimate the differential properties from a set of discrete noisy points can guarantee the accuracy of the estimated value. Being the property of a point set, Delaunay pole sphere is also invariant under any rigid body transformation with less deviation than any other intrinsic differential properties.

The proposed approach decreases the correspondence search dramatically by selecting only a reference triangle with three points from one object with specific properties and extracts the correspondent points having same properties from the second object. After the correspondence information is established, the iterative closest point (ICP) algorithm, whose effectiveness entirely relies on the correct initial correspondence information, is incorporated with the proposed algorithm to obtain a robust object

matching. The concept of *preprocessing* of the measurement data set is introduced before correspondence search is initiated. To combat the detrimental effect of the noise, a *point density reduction* approach has also been implemented.

Extensive simulations have been carried out to show the effectiveness of the proposed algorithm. An analysis of the simulation results demonstrate that a robust and efficient method of initial matching has been achieved when the prior information about the correspondence or transformation is not provided.

Keywords: Initial matching, Localization, Registration, Correspondence search, Delaunay pole sphere, Free-form surfaces, Rigid body transformation.

To my Family

Acknowledgements

Firstly, it is a delight to be able to express profuse and sincere thanks to my supervisor, Professor Hsi-Yung Feng, for his continuous support and invaluable guidance during my research work. He has been instrumental in the successful completion of this work and without his diligent research, intensive supervision, and unfathomable friendship this thesis would simply not have been possible.

I also gratefully acknowledge the indebtedness and express heartiest honor and sincere thanks to Dr. Daoshan OuYang under whose informative suggestions, heartily co-operation, patience, and encouragement the project work was carried out.

My stay at UWO is one of the most memorable moments of my life. I must also voice my heartfelt thanks to all my respective teachers, my fellow students of CAD/CAM/CAI research laboratory and my friends of UWO for making my stay here an enjoyable one.

Finally, enormous thanks are due to my beloved husband, Kamran for his constant love, patience and aspiration throughout my study. I am widely indebted to my parents and my sister for their untiring support throughout all of my academic endeavours. It is to them I dedicate this thesis.

Contents

List of Figures

List of Tables

Chapter 1

Introduction

The global demand on design and manufacturing of high precision products with complex sculptured surfaces has grown apace over the last decade and the growth is anticipated to continue over the next decade. The emergence in demand in design and manufacturing of increasingly sophisticated modern machinery necessitates the requisite advancement of Computer-Aided Design and Manufacturing (CAD/CAM) systems. The long-lasting attention devoted to this area can be traced to the large number of applications where almost all product data are created and stored in digital form using computer systems and directly provided as input to computer aided manufacturing systems to produce physical products. It is almost impossible to obtain a product with rigorous conformity to the specifications due to the ineluctable inaccuracy of the manufacturing process. In order to solve this problem, the designer introduces tolerances on each effective dimension of the product to be manufactured so that it can fulfill its function correctly. Inspection is the process that enables one to develop a comparison of a physical part to the specifications defined at the design stage.

To reduce time and cost, in industry, inspection is usually performed by human controllers based on a sampling of products rather than on the entire production.

Nevertheless, due to both the functional and aesthetic requirements of components and assemblies, particularly in automotive, aerospace and medical industries, all of the parts must be inspected because even the smallest defect is unacceptable and must be identified. The aim, therefore, is to incorporate automated inspection due to its main attractive features (e.g., consistency, repeatability, improved safety for inspectors, assessable criteria, and real-time operation).

1.1 Background and Motivation

In the CAD/CAM and graphics community, 3D model descriptions are typically described with CAD systems using digital data. The amplest shape variety can be modeled by *free-form* surfaces that are typically defined as *Non-Uniform Rational B-Spline* (NURBS) form which is widely accepted as an industry standard tool for the representation and design of product geometry [46]. NURBS is the mathematical representation of 3D geometry that can accurately describe any shape from a simple 2D line, circle, arc, or curve to the most complex 3D organic free-form surface or solid. Because of their flexibility and accuracy, NURBS models can be used in any process from illustration and animation to manufacturing.

Free-form surfaces and objects are often defined in intuitive rather than formal manner. In [13], Campbell and Flynn regarded free-*form* as a general characterization of an object whose surfaces are not of a more easily recognized class such as planar and/or natural quadratic surfaces. On the other hand, Besl [10] defined a free-form surface to be a smooth surface such that the surface normal is well defined and continuous almost everywhere, except at vertices, edges, and cusps. Since there is no other restriction on the

free-form surface, it is not constrained to be polyhedral or piecewise-quadric. Discontinuities in surface depth, surface normal or curvature may be present anywhere on the object and the curves that connect these points of discontinuity may meet or diverge smoothly [10]. The shape of the object can be arbitrary. Typical examples of representative objects with free-form surfaces used in manufacturing fields include ship hulls, marine propellers, automobile bodies, aircraft fairing surfaces, and biomedical replicated organs which can be represented in digital form using NURBS surface patches, polyhedral surfaces, and range data. Without the need to build an object prototype, CAD packages with capabilities to model free-form surfaces allow users to design, analyze, and test parts. Free-form surfaces are also applied in terrain modeling for cartographic applications. In this thesis, the terms "object with free-form surfaces" and "free-form objects" have been used interchangeably.

Although significant progress has been made in precision machining of free-form surfaces, inspection of surfaces remain a tedious job and has not been well studied [27]. The surface to be inspected can be measured by various ways such as using coordinate measuring machine (CMM) and laser scanner. Over the past few decades, coordinate measuring machines have found increasing demand as reliable devices for gathering dimensional data used in measurement and inspection applications. CMM, a contact device composed of electronic contact sensors, is the standard machine for the inspection of parts in industry as it is a flexible means of providing high-accuracy, high-throughput measurement, and is more cost effective than expensive custom gages used in many manufacturing operations. The CMM can also be fully automated and linked to a CAD system as well as used to measure and verify Geometric Dimensioning and Tolerancing

(GD&T) call outs. On the other hand, since the contact sensors can damage the surface of some product, the development of inspection system using computer vision sensors which are non-contact measurement devices is mandatory for the inspection of parts built of soft materials. A wide range of mold makers are adopting the emerging technology of 3D laser scanning in order to substantially reduce the time and cost of reverse engineering and inspection tasks. Optical systems, such as laser-based sensors, allow a great density of measurement points in a short time (more than 20,000 points per second) which drastically increases the inspection speed, whereas CMM are capable of much higher precision.

The measurement data obtained from CMM/laser scanner are required to be compared with the design model to determine whether the surface is out of tolerance. A critical issue in inspection is to align the design model and the manufactured part in time as closely as possible so that quality of that part can be examined properly online or offline. This process of aligning two objects is called *object matching*. Three dimensional object matching is a key issue in computer aided inspection, computer vision, and computer graphics. The term *registration* refers to matching when it is used in the areas of computer vision [11], whereas the term *localization* refers to matching when it is used in the areas of computer aided inspection [45]. Matching is employed in several applications. The localization technique is mostly applied for automatic inspection in the manufacturing process. Matching is important in machine vision for scene integration and object recognition, such as in medical image scanning (i.e., MRI), robotic autonomous navigation, and automatic production lines. It can also be used in the intellectual property protection of CAD model [33] and in congruence of different geometric representation.

Locating a part in a desire position and orientation and to maintain the position throughout the manufacturing process is also another significant application of object matching. Matching can also be applied in determining the relative altitude of a rigid object with respect to a reference.

Localization or registration aims at finding the best rigid body transformation which aligns two objects as closely as possible. The key factor in finding the best transformation in localization is the correspondence search between two surfaces. For matching of complex sculptured surfaces, many methods have been proposed so far. Minimization of a squared distance metric objective function of two objects is a commonly used matching method because of its ease and performance. But, for a case when no *a priori* information for the correspondence or initial transformation is available, which is generally the case, the direct distance minimization approach is of no use. The availability of the initial correspondence information is the key issue for the solution scheme to localization. An iterative search method can be employed to find the best transformation if and only if there is a good initial estimate of correspondence available. For this iterative process, correspondence can be provided by the user, but then it comes to the issue of human error, and the matching process does not provide the optimal solution. With no good initial estimate, the iterative approaches may end up being trapped in a local minimum so that a successful localization can not be obtained. Hence, only with the availability of very good initial information of the correspondence, a computationally efficient optimal localization can be obtained. In this thesis, we focus our attention to the problem pertaining to initial matching providing *a priori* information of the correspondence which has not been studied well so far.

1.2 Objectives

The objective of automated inspection system is to compare a finite sample of measurement data obtained from manufactured part with its design model such that the quality of the product can be verified under certain criteria. Performing inspection of manufactured product typically requires the following three stages: (i) a data capture stage which samples the 3D real world object in design model using the CAD software and the produced part to obtain the measurement data, (ii) a data localization stage which aligns the design model with the measurement data, and (iii) a data verification stage.

In order to qualify a part, the measurement data set is usually compared against the specified tolerance of the reference design model. Alignment of the product's design coordinate system with its measurement coordinate system is the best possible way to make the comparison. In the process of bringing the measurement surface and the corresponding design model in a common coordinate system, the design coordinate system is taken as the reference. How to locate the product's design coordinate system in the measurement coordinate system is the prime concern of the inspection process. The determination of positions and orientations of the design coordinate system of a part with respect to the measurement coordinate system is referred to as localization. The basic goal of localization is to find the best rigid body transformation parameters to align the two coordinate systems, which means to find the rotation matrix and translation vector between the coordinate frames. This process can be further explained by taking resort to the inspection model as shown in Figure 1.1 (modified version of figure [27]).

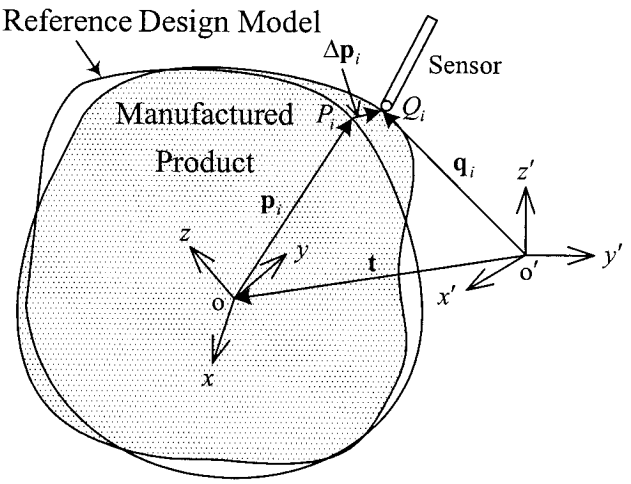

Figure 1.1: Schematic of the inspection model.

A measurement point Q_i in the measurement coordinate frame (x', y', z') denoted by the position vector $\mathbf{q}_i$ corresponds to the point P_i in the design coordinate frame (x, y, z) denoted by the position vector $\mathbf{p}_i$, where $i = 1, 2, \ldots, N$ and N is the number of points. Because of the manufacturing error, which happens in practice, the design coordinate frame does not coincide with the measurement coordinate frame. This is the reason behind the CAD data point P_i not being the same as the measurement data point Q_i. The relationship between the two frames can be represented by the following equation

$$\mathbf{q}_i = \mathbf{R}(\mathbf{p}_i + \Delta\mathbf{p}_i) + \mathbf{t} \tag{1.1}$$

where $\Delta\mathbf{p}_i$ is the distance between two surfaces at point $\mathbf{p}_i$; $\mathbf{R}$ is the rotational matrix and $\mathbf{t}$ is the translation vector from the reference design coordinate system to the compared measurement coordinate system. Since neither the rotation matrix and

translation vector nor the corresponding point set is known, the problem at hand can be formulated by the least-square approach. This leads the objective function given by

$$\min_{\mathbf{R},\mathbf{t}} \sum_{i=1}^{N} \left\| \mathbf{q}_i - (\mathbf{R}\mathbf{p}_i + \mathbf{t}) \right\|^2. \tag{1.2}$$

In minimizing this objective function, the information about the actual corresponding point sets is to be known.

To this end, the primary objective of the thesis is to develop an initial matching algorithm for automated inspection system to handle the point (sampled data from parametric surface such as NURBS surface) versus point (measurement data) cases when no *a priori* information on correspondence or initial transformation is available.

A computational geometric tool which exploits the property of the point density of the data set under investigation has been incorporated. In particular, Delaunay pole sphere, obtained from the computational geometric technique Delaunay triangulation [56], has been chosen as the localization tool because of its efficient and attractive properties to facilitate the correspondence search in performing object matching. A novel approach illustrating the preprocessing of data sets before initiating the proposed algorithm is also discussed. Figure 1.2 represents an overview of the proposed approach.

1.3 Literature Review

The problem of finding a match between three dimensional free-form objects attracted considerable research attention during the last decade. In this section, a summary of some of the previous work related to the areas of object matching is presented. This is not meant to be a comprehensive literature survey, but will provide the readers with the

background references on some of the ongoing research in the subject areas. This will yield a perspective on the techniques presented in this thesis.

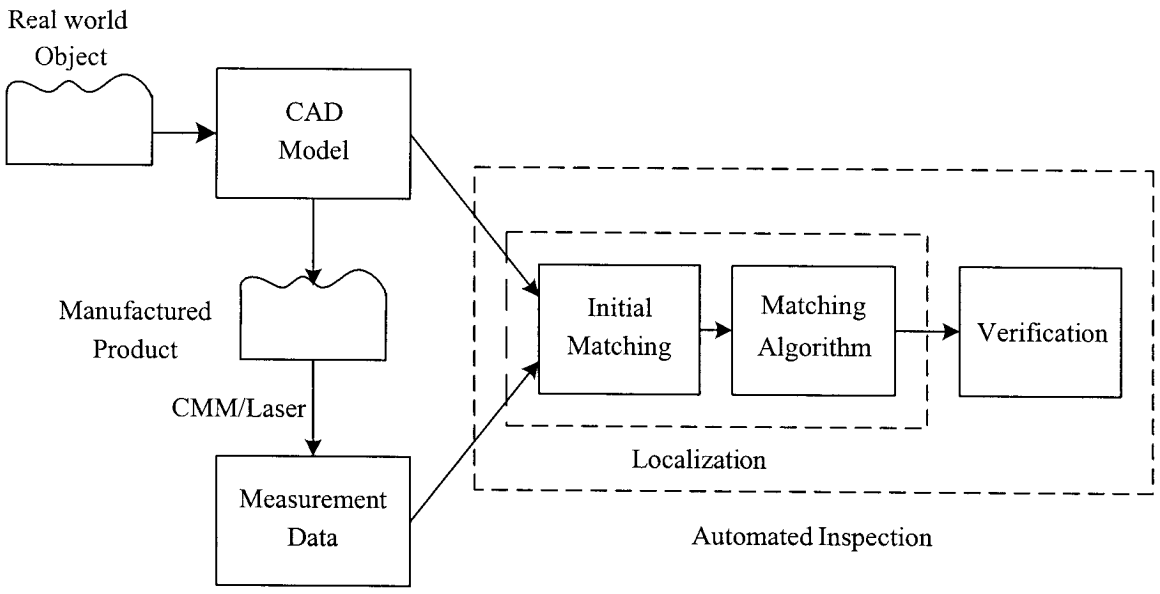

Figure 1.2: An overview of the proposed approach.

1.3.1 Matching with Known Correspondence

The correspondence search between two sculptured surfaces plays the major role in finding the best transformation to achieve the object matching. If such correspondence is known, transformation can be accomplished using closed form solution. An excellent overview regarding the problem of matching free-form surfaces can be found in [10]. One of the earliest significant approaches on registering two-free form surfaces was presented by Faugeras and Hebert [20]. They successfully applied the registration method to develop a system that recognizes and locates for the alignment of automobile parts in 3D space. In this method, model objects are represented in terms of linear features such as points, lines, and planes. The problem known as absolute orientation has several

closed-form, optimal solution methods in the literature. Absolute orientation seeks to align two sets of feature points, whose three-dimensional locations have been measured or reconstructed in two reference frames. Faugeras and Hebert [20] and Horn [24] proposed a closed-form solution for the least-square problem of absolute orientation. They employed quaternions to perform rigid body transformation between two coordinate systems given measurements of the coordinates of a set of points that are not collinear. The minimization of a cost function has been solved for rigid body transformation in a quadratic form of a unit quaternion which is a 4D vector that determines a 3D rotation matrix. The objective function in [24] is optimized with respect to rotation by finding the eigenvector corresponding to the maximum eigenvalue of a 4×4 matrix determined from centroid-referred point coordinates instead of the minimum eigenvalue. Walker *et al.* [57] interpreted the rotation quaternion in terms of the axis-angle representation by the *Euler Symmetric Parameters*. In other words, the orientation of the 3×1 vector component specifies the axis of rotation and the norm of the vector and scalar component are related to the rotation angle about this axis. Horn *et al.* [25] pointed out that these methods are not entirely novel, since the same problem had already been treated in the Psychometry (Quantitative Psychology) literature [50], [51] in the name of *Procrustes Analysis*. The method reported in [25] provides the rigid body transformation between two coordinate systems given measurements of the coordinates of a set of points that are not collinear using a matrix square-root solution.

Williams and Bennamoun [58] reported a new algorithm for performing the simultaneous rigid registration of multiple corresponding point sets. The minimization of a least-square cost function is proposed to solve the registration problem and it is also

shown that the cost function can be simplified to a quadratic expression involving unknown rotations and a constant matrix. The global point registration technique proposed in this paper is a generalization of the well known pairwise registration method reported by Arun *et al.* [5] which uses the singular value decomposition (SVD) to compute the optimal registration parameters in the presence of point correspondences. This approach gives a closed-form solution for the 3D rigid transformation between two 3D point sets. The method first reduces the unknown translation parameters, shifting all points to the center of gravity, and calculates the unknown rotation matrix using the SVD of a 3×3 matrix, finally computes the translation parameters. They also compared the difference of computation times between the techniques using the SVD, quaternions, and nonlinear iterations for the problem. Their results show that the computation time is about the same as using the SVD or the quaternions method whereas the iteration method takes a somewhat longer time. The primary limitation of this method is that it relies on the probable existence of reasonably large planar regions within a free-form shape. The techniques reported in [25] and [5] sometimes fail to provide a correct rotation matrix and give a reflection instead when the data are severely corrupted. However, if the points are not coplanar this is not a problem. Umeyama [55] provided modifications to [5] to ensure that a correct rotation matrix, instead of a reflection, is computed when the data are noisy. Another eigensystem is analyzed when the translation and rotation components are represented using *dual quaternions*[1.1] as reported in [57]. The motivation for the dual quaternions for estimating rigid transformation technique is that other rigid transformation estimation techniques first determine optimal orientation and thus use this

[1.1] A dual number is defined as $z = a + \varepsilon b$, where a, b are real numbers and ε is defined as $\varepsilon^2 = 0$, governing a special multiplication rule $(a + \varepsilon b)(c + \varepsilon d) = ac + \varepsilon(ad + bc)$.

solution to obtain translation (e.g., [5]), resulting in the accumulation of error in this computation. This approach solves for both relative orientation and position by minimizing a single cost function. With identical sets of point correspondences, the technique using dual quaternions provides similar accuracy to the SVD technique [5] for estimating rotation, but improved accuracy for estimating translation.

Sahoo and Menq [49] used tactile systems for sensing complex sculptured surfaces. They presented a method which determines position and orientation of an object by minimizing the sum of the squared distances of the measurement points from the surface of the object with respect to the parameters of transformation. Butler [12] provides a comparison of tactile methods and their performance. An obvious shortcoming of the method presented in [49] is that it needs to solve a set of six highly non-linear equations that requires an undesirable amount of computation time. The problem becomes worse for the case in which a large number of measurement data is required. To overcome this problem, a modified pseudoinverse-based algorithm called optimal match algorithm that aligns the measurement data with the design data in CAD-directed dimensional inspection is reported in [41]. This approach determines actual measured points by minimizing the sum of the squared distances of the measurement data from the surface of the part with respect to the parameters of a rigid body transformation. It has been shown that this modified algorithm is approximately 10 times faster than the algorithm reported in [49]. For many design and manufacturing engineering applications, free-form surfaces are often assigned a profile tolerance to control the variation. The inspection of a free-form surface is done by making an independent comparison between measured data and its design model with respect to its individual profile tolerance.

Inspection of this type of tolerance has been studied by a large number of researchers ([19], [22], [28], [30], [41], and [49]). An excellent review on this topic can be found in [35]. Some effort has been carried out to perform free-form surface inspection with a related profile tolerance. A system with a tolerance specification module and a comparative analysis module is reported in [29]. The free-form surface tolerances may have a relationship with more than one datum and the datum features may deviate from their designs. To resolve this situation, Huang and Gu extended their techniques and proposed the inspection of individual free-form surfaces [28] to the inspection of sculptured surfaces with design datums [27]. Recently, Li and Gu [36] proposed a localization technique based on two steps, firstly, they localize the measurement data to the CAD model based on the datum reference information and then depending on the information of the free-form surface, further localization is obtained. The correspondence search of the later step also entirely depends on the qualified datum feature information or the closest point concept. In another recent work [37], to establish the correspondence for localization, Li and Gu proposed the idea of surface feature extraction. They used the direction of mean and Gaussian curvature to define different types of free-form surface shapes. Most of the methods mentioned in this section are theoretically clear and also practical, but the correspondence must be established before the methods are applied.

1.3.2 Matching without Knowledge of Correspondence

The correspondence search between two object surfaces is a key issue in finding the best transformation for matching problem and a solution scheme for establishing correspondence depends on the availability of initial correspondence information. If such

correspondence is available, the problem at hand becomes trivial and the transformation can be easily computed using the algorithms based on methods such as unit quaternions [24] and least square fitting or the SVD approach [5], [41]. On the other hand, if knowledge about initial correspondence is not available, correspondence information between objects must be established to estimate the transformation. Once initial correspondence information is estimated accurately, an optimum transformation can be achieved through iteration by minimizing a mean square distance metric object function which involves six degrees of freedom for matching, such as the iterative closest point (ICP) algorithm [11], and its variants [53], [48]. The ICP algorithm is an iterative decent algorithm which can be applied to different data set including point, polygon, curve, and surface. The matching method is based on the search of the closest point from a point to a point set, a curve, or a surface, and utilizes the result to find two corresponding point sets. Then the unit quaternion method is used to find the rigid transformation between the two point sets. After that, the rigid transformation is applied to the points of one set and the process is repeated until the sum of squared distances is minimized. The ICP algorithm is based on the assumption that one point set is a subset of the other. When this assumption is not satisfied, mismatches happen which negatively influence the convergence of the ICP to correct solution [21]. To resolve this problem, several variations and improvements of the ICP method have been reported, e.g., in [40], [9], but there are still some unresolved problem. Exhaustive search for the nearest point makes this approach computationally expensive [52]. Another drawback of this method is that it requires every point in one surface to have a corresponding point on the other surface. As an alternative to this search problem, Chen and Medioni [15] proposed a technique to find

an optimal transformation based on estimated hypothetical transformations. This idea was originally reported in [47]. In [18], Dorai *et al.* extended the work of Chen and Medioni to an optimal weighted least-squares framework. They proposed and implemented a complete prototype system for registering and integrating multiple 3D object views from range data which can then be used to construct geometric models of the objects. Sharp *et al.* [53] generalizes the ICP algorithm to include Euclidean invariant features to provide a more effective algorithm. A similar approach proposed by Zhang [60] dealt with outlier, occlusion, appearance and disappearance incorporating a threshold technique using robust statistics to limit the maximum distance between points. The statistical analysis is utilized to filter out poorly matched data points.

Okatani and Deguchi [43] proposed a novel method for fine registration of two range images from different viewpoints taking into account the properties of the measurement error of the range data where the error distribution is different for each point in the image and is dependent on both the viewing direction and the distance to the object surface. Without any available information about correspondence, Bergevin *et al.* [7] proposed a technique to estimate the 3D rigid transformation between two range views of a complex object. In [8], Bergevin *et al.* proposed simultaneous registering of multiple range images to avoid the accumulation of the errors in the sequential estimation of transformation.

One stream of research considered some global properties of the object such as extended Gaussian image (EGI) [23], [32] and other orientation-based descriptors [42], [38], [39] which represents the 3D objects in terms of their surface-normal distributions on a unit sphere with appropriate support functions. Another stream of research reported

various complex surface representation schemes using some local properties of each point. They include the *splash* representation of Stein and Medioni [54], the *point signature* of Chua and Jarvis [14], the *shape spectrum* scheme of Dorai and Jain [17], the *surface signatures* from simplex meshes of Yamany *et al.* [59], the *harmonic shape images* of Zhang and Hebert [61], and the *spin image* representation proposed by Johnson and Hebert [31]. The method in [54] utilizes changes in surface orientation to match local patches of surfaces. Chua and Jarvis [14] formulated a new representation (the point signature) which follows along the same line as [54]. The point signature is different in that it does not encode information about the normals around the points of interest; rather it encodes the minimum distances of points on a 3D contour to a reference plane. In [31], pairwise registration is accomplished using spin images, an alternative representation for finding point correspondences. The final transformation is refined and verified using a modified ICP algorithm. The spin images are 2D histograms of the surface locations around a point. The spin images representation [31] is a 2D image that accumulates information about a surface patch while splashes [54] and point signatures [14] are 1D representations that accumulate surface information along a 3D curve. Because these local properties encode the coordinates of points on the surface of an object with respect to a local basis, it is a local description of the global shape of the object and is invariant to rigid transformation. All these methods require extensive computational searches among the correspondence possibilities between two objects' points which are not practical for real time processing.

Recently, Ko *et al.* [33] proposed a method to use three non-collinear points with different curvature values in one object and their possible correspondent points in another

object to decrease the possibilities search. They developed a global matching method to handle the point vs. NURBS surface and the NURBS surface vs. NURBS surface cases when no *a priori* information on correspondence or initial transformation is provided. Matching is performed by using two intrinsic surface properties, the Gaussian and the mean curvature, as object features. With rough tolerances, this method uses the ICP algorithm to obtain refined localization. The main deficiency of this algorithm is that it can deal only with the point vs. surface or surface vs. surface matching cases so that it can not be used for free-form objects in discrete data points. Moreover, since they are using the mean and Gaussian curvature for correspondence search, while dealing with the point vs. surface case, estimation of curvature from a set of discrete data points is needed. Being a second order differential property, curvature is sensitive to the corrupted data. So, accurate estimation of curvatures values from a set of data with noise is almost impossible. No estimation method used to estimate the curvatures can guarantee the accurate value for curvature, since the accuracy depends on the estimation method, the digitization devices etc. For the solution of this curvature estimation problem, Ko *et al.* suggested scanning a region around a point several times and then to use the curvature estimation method, which is not a practical solution and can not guarantee the accuracy of the estimation method either.

Taking these into consideration, a novel approach for robust initial matching of free-form objects represented by point cloud data providing optimal initial estimation of transformation or correspondence is provided. Delaunay pole sphere has been employed as the localization tool in this work with great efficiency instead of any intrinsic properties of the shape.

1.4 Organization of the Thesis

This thesis is concerned with *localization* which is a generic problem in the Computer-Aided Inspection (CAI). This localization problem consists of the matching of the CAD model of an object with its measurement data set to verify the quality of the product.

The thesis is organized as follows. In the first Chapter, the work has been motivated in the context of initial object matching. A brief review of the available literature is given on the problems of matching 3D sculptured surfaces with and without any initial information of correspondence or transformation. In Chapter 2, the fundamental concepts and methods to compute rigid body transformations (rotation and translation) as well as the overview of the ICP algorithm is provided.

Chapter 3 introduces Delaunay pole sphere, a new invariant property, as the localization tool and describes the method of its construction. The reasons for choosing this property as an effective tool for the proposed initial matching algorithm have also been discussed. In Chapter 4, the concept of *preprocessing* of the measurement data set before initiating the correspondence search for the proposed approach is introduced.

The proposed initial matching algorithm providing estimated transformation parameters to achieve free-form object matching without the availability of initial correspondence information is presented in Chapter 5. The details of the approach along with its implementation technique have also been discussed. Chapter 6 shows extensive simulation results to evaluate the performance of the proposed algorithm.

Finally, it is concluded in Chapter 7 with the major contributions of the thesis and the avenues for further research.

Chapter 2

Relevant Mathematical Principles

The basic goal of localization or registration is to find the best rigid body or Euclidean transformations which align two free-form objects as closely as possible. A unique property of these transformations is that they preserve the shape of the objects that they act on. In the context of this thesis, rigid body transformations consist only of translations and rotations which correspond intuitively to our notions of real rigid bodies which can not be scaled or stretched in any way.

The main challenges of the problem lie in identifying an objective function that can quantify the quality of the alignment between the objects and in defining a procedure to modify and refine current estimates of the transformation parameters in a way that the similarity measure or the objective function is optimized. The primary goal in this chapter is to introduce all the important definitions and approaches associated with the estimation of rigid body transformations that can be useful in the sequel. ICP algorithm is incorporated in our proposed initial matching approach for performing localization of rigid 3D shapes after correspondence information between objects is established. The overview of the ICP algorithm will also be introduced in this chapter.

2.1 Rigid Body Transformations

A *rigid body* is an object which is a collection of particles/points such that the distance between any two particles/points remains fixed, regardless of any motions of the object or transformations applied on the object. Hence, if $\mathbf{a}(t)$ and $\mathbf{b}(t)$ are two points on a rigid body at time t, $\mathbf{a}$ and $\mathbf{b}$ must satisfy the following conditions as the object moves.

$$\|\mathbf{a}(t)-\mathbf{b}(t)\| = \|\mathbf{a}(t-1)-\mathbf{b}(t-1)\| = \|\mathbf{a}(0)-\mathbf{b}(0)\| = \text{constant}. \qquad (2.1)$$

A *rigid motion* of an object is a continuous movement of the points in the object such that the distance between any two points remains fixed at all times. The net movement of a rigid body from one place to another via a rigid motion is called a *rigid displacement*. Generally, a rigid displacement may consist of both translation and rotation of the object. A *translation* can be thought of as a transformation consisting of a constant offset or sliding, with no rotation or distortion, of an object from one position to another. A composite of two (or any even numbered) reflections over parallel lines will result in a translation. In n dimensional Euclidean space, a translation is simply specified as a vector giving the offset in each of the n coordinates. On the other hand, a transformation is a *rotation* if and only if it is the composite of two successive reflections through intersecting lines. A rotation is an orientation-preserving[2.1] orthogonal transformation such that the object turns by an angle about a fixed point.

Let us consider an object which can be described as a subset $\boldsymbol{O}$ in $\boldsymbol{R}^3$. Considering two points $\mathbf{a}, \mathbf{b} \in \boldsymbol{O}$, the vector $\mathbf{k} \in \boldsymbol{R}^3$ connecting $\mathbf{a}$ to $\mathbf{b}$ is given by $\mathbf{k} = \mathbf{b} - \mathbf{a}$. Naturally, the action of a rigid transformation on points of an object induces an

[2.1] A nonsingular linear map $f : \boldsymbol{R}^n \to \boldsymbol{R}^n$ is orientation-preserving if $\det(f) > 0$.

action on vectors. If a map $f : \boldsymbol{O} \rightarrow \boldsymbol{R}^3$ represents a rigid displacement, then vector transform according to

$$f_*(\mathbf{k}) = f(\mathbf{b}) - f(\mathbf{a}). \tag{2.2}$$

Since rigid motions do not alter distances between points on a rigid body, a necessary condition for a mapping $f : \boldsymbol{O} \rightarrow \boldsymbol{R}^3$ to represent a rigid motion is that distances be preserved by the mapping. However, this condition is not sufficient since it allows internal reflections, which are not physically realizable. Hence, a mapping might preserve distance but not the orientation. For example, the mapping $[x, y, z] \rightarrow [x, y, -z]$ preserves distances but reflects points in the body about the xy plane. In order to avoid this possibility, it is required that the cross product between vectors in the object also be preserved. To this end, the concept of rigid body transformation comes into the mind. A mapping $f : \boldsymbol{R}^3 \rightarrow \boldsymbol{R}^3$ is a *rigid body transform* if it satisfies the following properties:

1. Length is preserved, i.e., $\|f(\mathbf{a}) - f(\mathbf{b})\| = \|\mathbf{a} - \mathbf{b}\| \quad \forall\, \mathbf{a}, \mathbf{b} \in \boldsymbol{R}^3$.
2. The cross product is preserved, i.e., $f_*(\mathbf{k} \times \mathbf{u}) = f_*(\mathbf{k}) \times f_*(\mathbf{u}) \quad \forall\, \mathbf{k}, \mathbf{u} \in \boldsymbol{R}^3$.

Rigid body transformation restricts the searched transformation to be a combination of translations and rotations which are sufficient to describe the movement of rigid objects.

The accurate estimation of 3D rigid body transformations builds the basis for object matching techniques. To this end, Arun *et al.* [5] proposed a well known pairwise localization method which gives a closed-form solution for the 3D rigid body transformation between two 3D point sets. This method uses the SVD technique to compute the optimal localization parameters in the presence of point correspondences. To avoid the possibilities of reflections, another approach based on unit quaternions [24] is

preferred over SVD approach in two and three dimensions which also gives an optimal closed-form solution. However, the SVD approach can be generalized to n dimensions and would be the method of choice for $n > 3$ in any $n-$dimensional applications. A give brief overviews of these approaches is given in this section.

2.1.1 SVD Approach

Two free-form objects to be matched can be described as point sets denoted by $X = \{\mathbf{x}_1, \mathbf{x}_2, \ldots, \mathbf{x}_N\}$ and $Y = \{\mathbf{y}_1, \mathbf{y}_2, \ldots, \mathbf{y}_N\}$ assuming that the correspondence of the point sets are known or established earlier. $\mathbf{x}_i$ and $\mathbf{y}_i$, $\{i = 1, 2, \ldots, N\}$, are considered to be 3×1 column vector. The points in the two objects with the same subscript mean that they represent 3D correspondences. Given the localization parameters 3×3 rotation matrix $\mathbf{R}$ and 3×1 translation vector $\mathbf{t}$, any point $\mathbf{x}_i$ in the first object is related to its corresponding point $\mathbf{y}_i$ in the second object according to the following relation

$$\mathbf{y}_i = \mathbf{R}\mathbf{x}_i + \mathbf{t}. \tag{2.3}$$

The aim of the problem at hand is to find the rotation matrix $\mathbf{R}$ and translation vector $\mathbf{t}$, which minimize the following objective function

$$\min_{\mathbf{R},\mathbf{t}} \sum_{i=1}^{N} \left\| \mathbf{y}_i - (\mathbf{R}\mathbf{x}_i + \mathbf{t}) \right\|^2. \tag{2.4}$$

The problem can be reformulated in a manner which decouples the computation of $\mathbf{t}$ from that of $\mathbf{R}$ by referring the coordinates to the respective centroids of each point set. Let $\hat{\mathbf{R}}$ and $\hat{\mathbf{t}}$ be the least-squares solution to (2.3). It has been shown in [26] that $\{\mathbf{y}_i\}$ and $\{\mathbf{x}'_i := \hat{\mathbf{R}}\mathbf{x}_i + \hat{\mathbf{t}}\}$ have the same centroid. Hence, it gives

$$\bar{\mathbf{y}} = \bar{\mathbf{x}}' \tag{2.5}$$

where

$$\bar{\mathbf{y}} = \frac{1}{N}\sum_{i=1}^{N}\mathbf{y}_i \tag{2.6}$$

$$\bar{\mathbf{x}} = \frac{1}{N}\sum_{i=1}^{N}\mathbf{x}_i \tag{2.7}$$

$$\bar{\mathbf{x}}' = \frac{1}{N}\sum_{i=1}^{N}\mathbf{x}_i' = \hat{\mathbf{R}}\bar{\mathbf{x}} + \hat{\mathbf{t}}. \tag{2.8}$$

Defining

$$\mathbf{g}_i := \mathbf{x}_i - \bar{\mathbf{x}} \tag{2.9}$$

$$\mathbf{h}_i := \mathbf{y}_i - \bar{\mathbf{y}} \tag{2.10}$$

equation (2.4) turns into the following minimizing problem

$$\min_{\mathbf{R},\mathbf{t}} \sum_{i=1}^{N} \left\| \mathbf{h}_i - \mathbf{R}\mathbf{g}_i \right\|^2. \tag{2.11}$$

In this way the original problem is resolved into two parts. The first is to find $\hat{\mathbf{R}}$ to minimize (2.11) and the second is to estimate $\hat{\mathbf{t}}$ as given by

$$\hat{\mathbf{t}} = \bar{\mathbf{y}} - \hat{\mathbf{R}}\bar{\mathbf{x}}. \tag{2.12}$$

The SVD algorithm for computing $\hat{\mathbf{R}}$ is based on the singular value decomposition of a 3×3 matrix as explained below. After calculating $\bar{\mathbf{x}}$, $\bar{\mathbf{y}}$, $\{\mathbf{g}_i\}$, and $\{\mathbf{h}_i\}$ a 3×3 matrix is computed defined by

$$\mathbf{H} := \sum_{i=1}^{N} \mathbf{g}_i \mathbf{h}_i^T \tag{2.13}$$

where the superscript $(\cdot)^T$ denotes the transpose operator. Next, the SVD of $\mathbf{H}$ is computed given by

$$\mathbf{H} = \mathbf{U}\sum\mathbf{V}^T. \tag{2.14}$$

After computation of the SVD, a new 3×3 matrix $\mathbf{D}$ is formed as

$$\mathbf{D} = \mathbf{V}\mathbf{U}^T. \tag{2.15}$$

Finally, the determinant of $\mathbf{D}$, $\det(\mathbf{D})$ is calculated.

If the $\det(\mathbf{D}) = +1$, then estimated rotation matrix $\hat{\mathbf{R}}$ is set equal to $\mathbf{D}$, and solved for $\hat{\mathbf{t}}$ as noted previously. If the determinant of $\mathbf{D}$ is negative, then it indicates the situation of reflection and the algorithm fails. The reader is referred to the original paper [5] for more details and proof of the SVD algorithm to accomplish pairwise localization.

2.1.2 Unit Quaternions Approach

A quaternion can be thought of as a generalization of a complex number with a real part and three different imaginary parts or as a composite of a 3×1 vector and a scalar. Mathematically, the unit quaternion can be defined as a 4D vector

$$\mathbf{q} \coloneqq [q_0, q_1, q_2, q_3]^T \tag{2.16}$$

where $q_0 \geq 0$ and $q_0^2 + q_1^2 + q_2^2 + q_3^2 = 1$. The quaternion representation makes the minimization of (2.4) equivalent to the maximization of a quadratic form of a unit quaternion [24]. The optimal rotation matrix is formed from the unit quaternion that is the unit eigenvector corresponding to the most positive eigenvalue of a 4×4 matrix whose components are generated from the cross-covariance matrix between the given pairs of point sets. Using (2.6) and (2.7), the cross-covariance matrix $\mathbf{Q}_{xy}$ of the point sets X and Y is given by

$$\mathbf{Q}_{xy} = \frac{1}{N}\sum_{i=1}^{N}\left[(\mathbf{x}_i - \bar{\mathbf{x}})(\mathbf{y}_i - \bar{\mathbf{y}})^T\right] = \frac{1}{N}\sum_{i=1}^{N}\left[\mathbf{x}_i\mathbf{y}_i^T\right] - \bar{\mathbf{x}}\bar{\mathbf{y}}^T. \tag{2.17}$$

Next, the cyclic components of the anti-symmetric matrix $B_{ij} = [\mathbf{Q}_{xy} - \mathbf{Q}_{xy}^T]_{ij}$ are used to form a column vector given by $\Delta = [B_{23}, B_{31}, B_{12}]^T$. By using this vector, a symmetric 4×4 matrix is formed as

$$\mathbf{S} = \begin{bmatrix} \mathrm{tr}(\mathbf{Q}_{xy}) & \Delta^T \\ \Delta & \mathbf{Q}_{xy} + \mathbf{Q}_{xy}^T - \mathrm{tr}(\mathbf{Q}_{xy})\mathbf{I}_3 \end{bmatrix} \tag{2.18}$$

where $\mathrm{tr}(\cdot)$ indicates trace of a matrix and $\mathbf{I}_3$ is the 3×3 identity matrix. Finally, eigen decomposition of the matrix $\mathbf{S}$ is computed. The unit eigenvector corresponding to the maximum eigenvalue of $\mathbf{S}$ represents the unit quaternion $\mathbf{q} = [q_0, q_1, q_2, q_3]^T$ which is used to derive optimal 3×3 rotation matrix given by

$$\hat{\mathbf{R}}_{\mathrm{opt}} = \begin{bmatrix} q_0^2 + q_1^2 - q_2^2 - q_3^2 & 2(q_1 q_2 - q_0 q_3) & 2(q_1 q_3 + q_0 q_2) \\ 2(q_1 q_2 + q_0 q_3) & q_0^2 + q_2^2 - q_1^2 - q_3^2 & 2(q_2 q_3 - q_0 q_1) \\ 2(q_1 q_3 - q_0 q_2) & 2(q_2 q_3 + q_0 q_1) & q_0^2 + q_3^2 - q_1^2 - q_2^2 \end{bmatrix}. \tag{2.19}$$

The optimal translation vector $\hat{\mathbf{t}}_{\mathrm{opt}}$ is obtained by the difference between the transformed centroids of the first point set and the second one. Hence,

$$\hat{\mathbf{t}}_{\mathrm{opt}} = \bar{\mathbf{y}} - \hat{\mathbf{R}}_{\mathrm{opt}} \bar{\mathbf{x}}. \tag{2.20}$$

This approach uses only the centroids and the cross-covariance matrix of the given pair of point sets, and it gives a closed-form solution if more than three pairs of points are given. We use this approach in our proposed algorithm to compute optimal transformation parameters, after establishing the correspondences between the point sets.

The above two methods give closed-form solution if and only if the correspondences between the point sets are known. We present next a widely used

algorithm to estimate transformation parameters between paired 3D shapes without preliminary correspondences.

2.2 Iterative Closest Point Algorithm

Up to now, several approaches have been proposed for 3D data localization. The iconic algorithm introduced by Besl and McKay [11] is a standard solution to the general purpose problem for the localization of rigid 3D shapes without preliminary point correspondences, which they refer to as the *iterative closest point* (ICP) algorithm. Rusinkiewicz and Levoy [48], who suggested that *iterative correspondence point* is a better expansion for the abbreviation of the ICP than the original *iterative closest point*, presented an excellent summary with new results on the acceleration of the ICP algorithm. The ICP algorithm is composed of two different procedures:

1. Search of the corresponding point and hence, generation of the temporary point correspondences, and
2. Estimation of the 3D rigid transformations from the point correspondences.

These two procedures are iterated until the two given shapes are localized by the estimated transformation matrix. ICP starts with two point sets and an initial guess for their relative rigid body transformation, and iteratively refines the transformation by repeatedly generating pairs of corresponding points from the point sets and minimizing an error metric.

We consider two independently derived sets of 3D points which correspond to a single shape. The algorithm aims a measurement point set (the *data* set D) of N_d points, $\{\mathbf{d}_1, \mathbf{d}_2, \ldots, \mathbf{d}_{N_d}\}$ is rigidly transformed to be in best alignment with the corresponding

CAD model (the *model* set M) of N_m points, $\{\mathbf{m}_1, \mathbf{m}_2, \ldots, \mathbf{m}_{N_m}\}$. Let $\|\mathbf{d}-\mathbf{m}\|$ be the Euclidean distance between points $\mathbf{d} \in D$ and $\mathbf{m} \in M$. For each point $\mathbf{d}_i$, $\{i = 1, 2, \ldots, N_d\}$ there exists at least one point on the surface of M which is closer to $\mathbf{d}_i$ than any other points in M. This is the closest point $\mathbf{m}_i$. The basic idea behind the ICP algorithm is that under certain conditions, the point correspondence furnished by sets of closest points is the approximation to the true point correspondence which is not plausible for many practical situations, specifically when data sets are transformed in a random manner. Moreover, ICP algorithm considers an identity matrix as the initial transformation information to transform the measurement data which means that the algorithm starts with two original raw data sets without any transformation. Hence, the first updated new data set can be expressed as $D_{new} = D$. The ICP algorithms depicted in Figure 2.1 can be summarized as follows:

Step 1. For each data point in D_{new}, the closest point on the surface of the CAD model M is computed. Consequently, a point sequence $\{\mathbf{m}_1, \mathbf{m}_2, \ldots, \mathbf{m}_{N_d}\}$ in M to the data point sequence $\{\mathbf{d}'_1, \mathbf{d}'_2, \ldots, \mathbf{d}'_{N_d}\}$ in D_{new} can be obtained where each point $\mathbf{d}'_i$, $\{i = 1, 2, \ldots, N_d\}$ corresponds to the point $\mathbf{m}_i$, $\{i = 1, 2, \ldots, N_d\}$ with the same index.

Step 2. With the correspondence established from Step 1, the transformation matrix $\mathbf{T}$ is computed such that the transformed data points $\mathbf{T}(\mathbf{d}_i)$ are closest to their corresponding points $\mathbf{m}_i$, where the objective function turns into the

minimizing problem given by

$$\min_{\mathbf{T}} \sum_{i=1}^{N_d} \left\| \mathbf{m}_i - \mathbf{T}(\mathbf{d}_i) \right\|^2. \tag{2.21}$$

This least squares problem can be solved explicitly, see e.g., [24], [11]. An overview of the computation of the rigid body transformation was presented in previous section.

Step 3. The transformation obtained from Step 2 is applied to the original data in D i.e., the points in data set are updated via $D_{\text{new}} = \mathbf{T}(D)$.

Step 4. Step 1-3 are repeated, as long as the change in mean-square error (MSE) falls below a preset positive threshold τ. The MSE is computed between points in D_{new} and the corresponding closest points of the CAD model.

Instead of seeking real physical correspondences, the ICP algorithm tries to search the correspondence between data point sets by finding closest points iteratively. This affects the computation of the optimum transformation using the algorithm based on the known correspondences of the data sets. Since ICP is a non-linear local search algorithm, it suffers from many problems commonly associated with local searches, such as slow convergence and the tendency to fall into local minima. The ICP algorithm always converges monotonically to a local minimum with respect to the mean-square distance objective function [11]. It requires a good initial transformation to converge acceptably. To solve this problem, we take resort to the Delaunay pole sphere, a computational geometric tool invariant under any rigid body transformations, to establish the effective point correspondence information for achieving efficient initial matching.

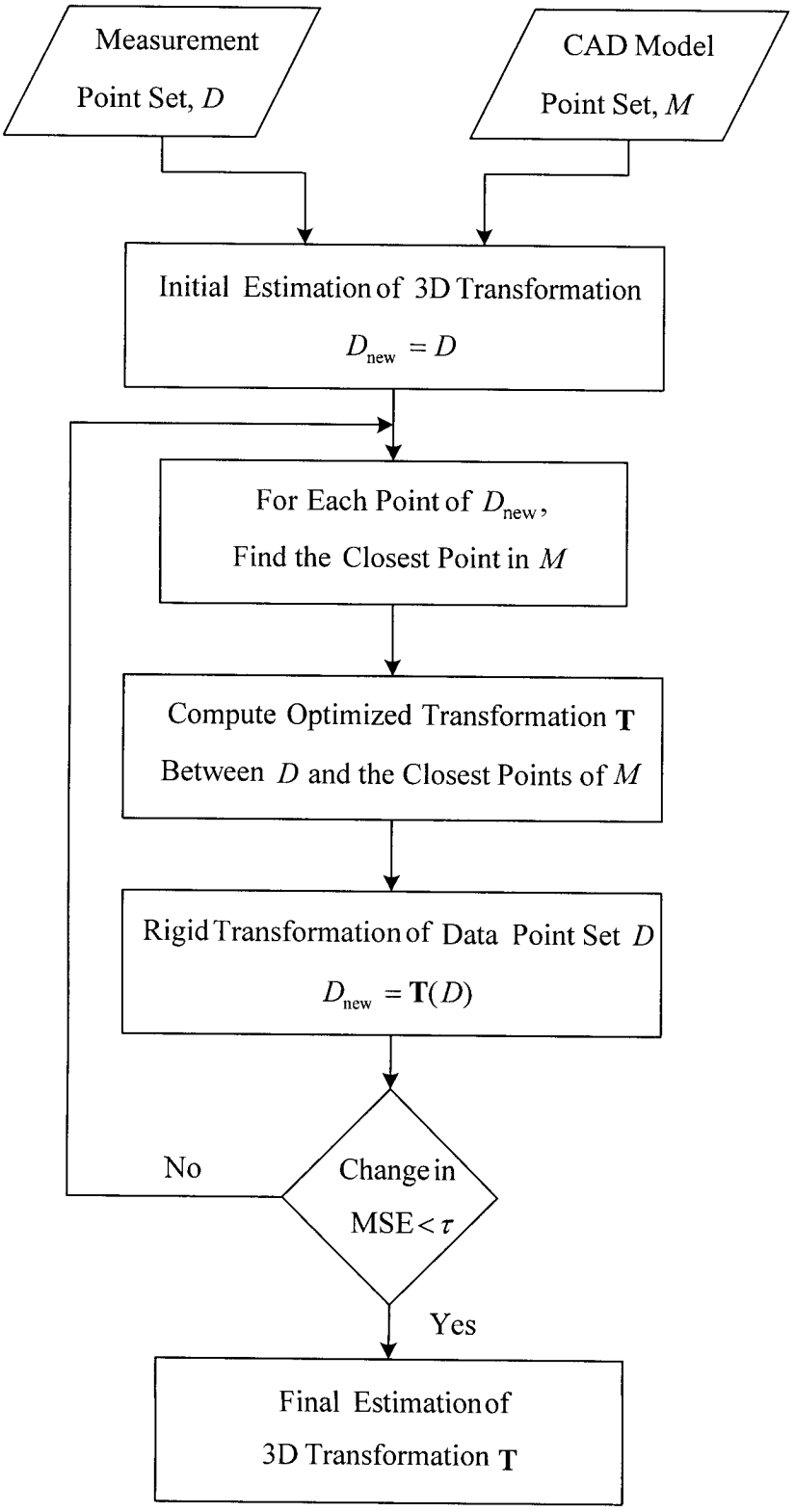

Figure 2.1: Flowchart of the ICP algorithm.

Chapter 3

Delaunay Pole Sphere: The Localization Tool

The efficacious computational geometric tool that has been used in the proposed algorithm for initial matching of two point cloud data is the Delaunay pole sphere. Since it is necessary to establish the correspondence relationship between the input point sets, an optimal property of those point sets has been used to extract the required correspondence information. This property comes from the omnipresent Voronoi diagram and its geometric dual, the Delaunay triangulation [56]. These well known algorithms are the fundamental topics in computational geometry and have been rediscovered or applied in many applications because of their unique and predictable outcomes. This Chapter introduces the basic concept of the computational geometric techniques and the new invariant property, Delaunay pole sphere, derived from those techniques. The reasons for choosing this property as an effective tool for initial matching pertaining to the proposed algorithm have also been discussed.

3.1 Voronoi Diagram

Voronoi diagram has different applications in many practical fields as well as within the field of computer science, in particular, computational geometry. A Voronoi diagram of a set of points is a collection of regions that divide up the plane. The Voronoi diagram can be considered as a set of convex polygons in two dimension, and convex polyhedron in three dimension where each Voronoi region is termed as cell. Each input point, which is commonly referred to as site, is contained within a cell and every spatial location within that cell is closer to that site than to any other site in the set. Figure 3.1 is the depiction of a two dimensional example of a Voronoi diagram.

For mathematical representation of the concept of Voronoi diagram, let

$$P := \{\mathbf{p}_1, \mathbf{p}_2, \ldots, \mathbf{p}_n\} \tag{3.1}$$

be defined as a set of n distinct points in the plane. The Voronoi diagram of P is the subdivision of the plane into n cells, one for each site in P, with the property that a point $\mathbf{q}$ lies in the cell corresponding to a site $\mathbf{p}_i$, $\{i = 1, 2, \ldots, n\}$ if and only if

$$\text{dist}(\mathbf{q}, \mathbf{p}_i) < \text{dist}(\mathbf{q}, \mathbf{p}_j) \text{ for each } \mathbf{p}_j \in P \text{ with } j \neq i \text{ and } \{j = 1, 2, \ldots, n\} \tag{3.2}$$

where dist(.,.) represents the Euclidean distance between the two points of its argument. The boundary between two adjacent regions which is called the Voronoi edge is a line segment and this edge is the perpendicular bisector of the segment joining the two sites. Each of the cell vertices has at least four equidistant sites in 3D.

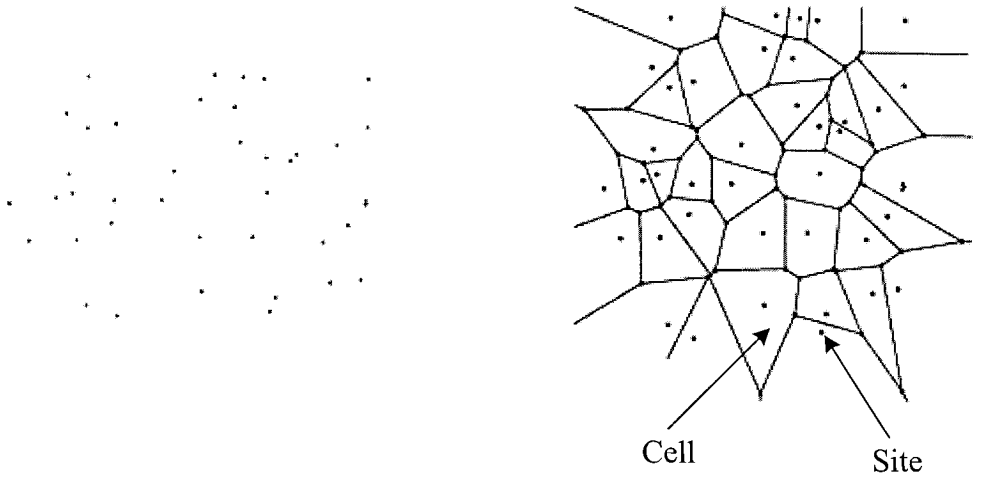

Input points Voronoi diagram of the input point sets

Figure 3.1: 2D representation of a Voronoi diagram.

3.2 Delaunay Triangulation

A well known topic of computational geometry which is also known in various fields is the problem of triangulating a set of points. Among all the triangulation methods used, Delaunay triangulation, the geometric dual of the Voronoi diagram, is the most widely used one. It has several practical implementations such as height interpolation and mesh generation. For a set of input points, the Delaunay triangulation is an extension of the Voronoi diagram with a different emphasis placed on the set of input sites. Instead of being partitioned into cells, the sites of Delaunay triangulation become the vertices of triangles in two dimensions and of tetrahedrons in three dimensions. In Delaunay triangulation, the vertices of the triangle specify a circum-circle in 2D, whereas the vertices of tetrahedron specify a circum-sphere in 3D that contains no other sites in the set. Therefore, the vertices of each Voronoi cell become the centres of Delaunay spheres. The calculation of the circum-sphere of the tetrahedron is described in Appendix A.

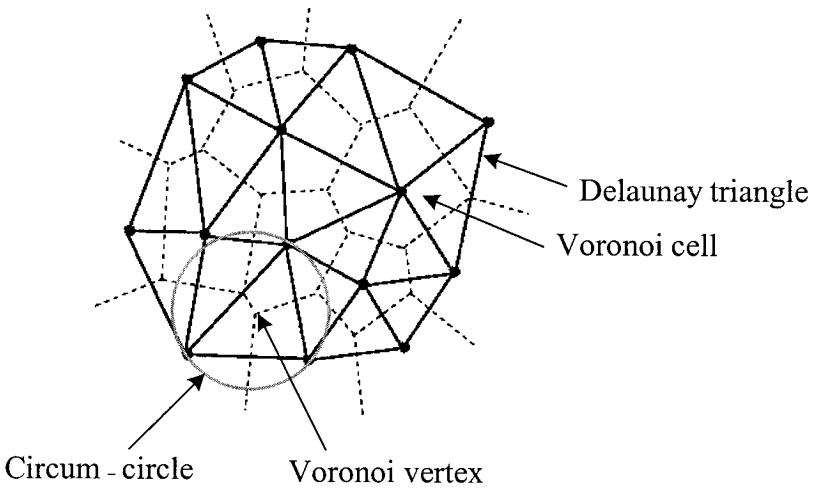

Figure 3.2: Depiction of Delaunay triangulation, Voronoi diagram, and the circum-circle.

Figure 3.2 represents the combined view of Delaunay triangulation and Voronoi diagram to describe their interrelationship, and the circum-circle at Voronoi vertex. The Quick hull algorithm [6] is used in this thesis for the calculation of the Delaunay triangulation and Voronoi diagram by considering its efficiency. Because of being dual, computing either the Delaunay triangulation or the Voronoi diagram automatically gives the other one. This Quickhull algorithm used for the calculation of Delaunay triangulation is taken from the publicly available C++ code of CGAL (Computational Geometry Algorithms Library) [62].

3.3 Delaunay Pole Sphere

In Delaunay triangulation, the vertices of the Delaunay tetrahedron form Delaunay sphere that contains no other sites inside the sphere. Amenta *et al.* [3] introduced the concept of poles which are a subset of the Voronoi vertices of the point set. Each site is associated with two poles which are defined as the furthest vertices of each Voronoi cell that lie on

each side of the surface. But they mentioned in their later work [4] that their surface reconstruction algorithm does not work well for sharp edges. This is because the Voronoi cell of a sample point set on a sharp edge is not long and thin so that the assumption under which they choose the poles for sharp edges is not correct. To this end, a new pole construction method is proposed for this work.

To accomplish the pole construction, the Delaunay cell clustering method proposed by OuYang and Feng [44] is implemented because of its simplicity and efficiency. Triangular mesh has been constructed using this method as it treats the points from corner area and the points from sharp area in the same manner whereas most of the surface reconstruction methods fail to reconstruct mesh properly while dealing with randomly sampled points. For each site, the incident Delaunay spheres are divided into two groups by its closed local Delaunay triangular mesh. The separation of the Delaunay spheres occurs along the curve or surface as the point density increases. This separation results all the Delaunay spheres for each point to be clustered into two groups. From each group, the Delaunay sphere of maximum size is estimated and will be referred to as Delaunay pole spheres hereinafter. Being a property of the point set, Delaunay pole sphere is invariant under any rigid body transformation which makes it an efficient tool for object matching. In this thesis, the Delaunay pole spheres are used with great efficacy.

3.4 Medial Axis

In recent years, potential use of medial axis in various geometric modeling applications has received a great deal of attention. The work has been driven by a wide variety of

interest and areas of applications such as image processing, computer vision, solid modeling, and mesh generation as a skeleton shape representation [16].

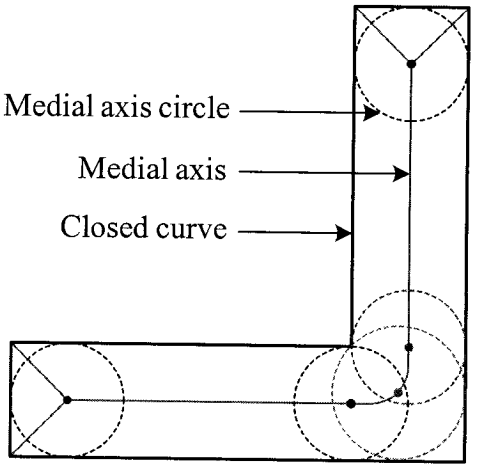

Figure 3.3: Representation of the medial axis and the medial axis circle of a closed curve.

The medial axis of a geometric object in 3D, also referred to in the literature as the skeleton, is defined as the locus of centers of the theoretical maximum empty spheres at each site. More generally, the medial axis of a shape is the group of centers of spheres that touch at least two points of the surface of the object. The theoretical maximum empty sphere, termed as a *medial axis sphere*, is the one which does not have any other part of the surface contained within it, and have their centres along the normal direction of the surface at every site and touch at least one other site on the surface. A closed curve, its medial axis, and the maximum empty circles within it are represented in Figure 3.3.

3.5 Reasons for Selecting Delaunay Pole Sphere

This section focuses on the reasons for selecting Delaunay pole spheres as the localization tool used in the proposed approach to accomplish the initial matching.

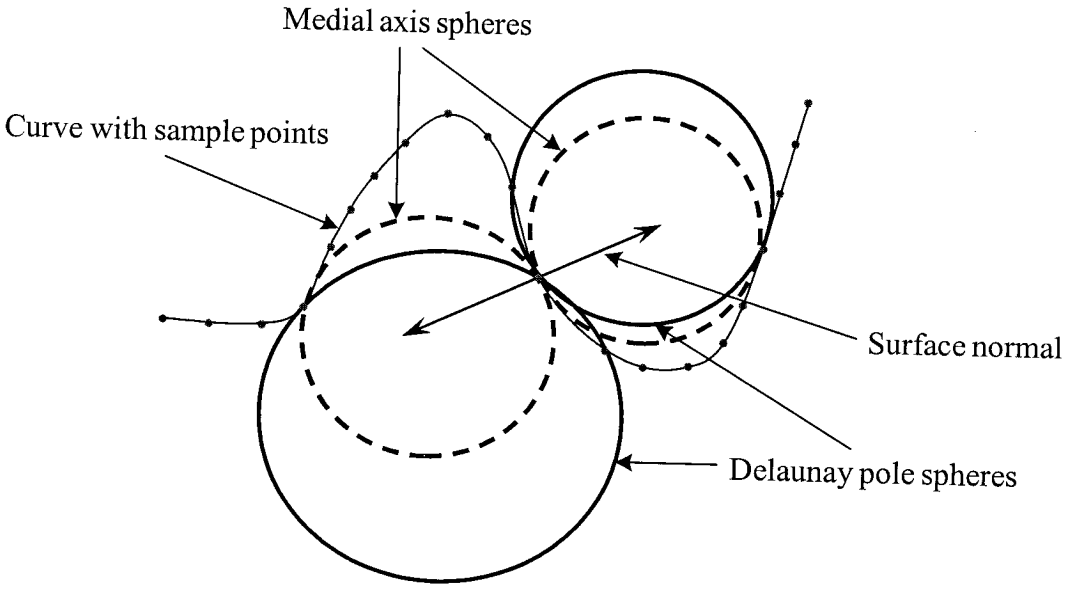

Figure 3.4: Representation of Delaunay spheres and corresponding medial axis of a site.

3.5.1 Medial Axis Approximation

Even though the medial axis provides the theoretical representation of the shape of a surface, there are no robust algorithms currently available that can generate the exact medial axes of all shapes and thus the corresponding sphere radii are difficult to obtain. Hence, it is difficult to construct the medial axis of a shape in three dimensions.

In many instances, the Delaunay pole spheres have been used to approximate the medial axis spheres e.g., [2], although the validity of this approximation can not be guaranteed because of the possibility of their centres being arbitrarily far from each other [3]. Figure 3.4 represents the interrelationship between the Delaunay pole spheres and the corresponding medial axis spheres in two dimensions.

When the sample points are sufficiently dense, the concept of pole introduced by Amenta and Bern [3] is almost similar to our concept of pole used in this research work. According to [1], for sufficiently dense sample points, the Voronoi cell of every sample

point appears naturally long and slim, and is approximately perpendicular to the boundary of the object which is represented in Figure 3.5 modified from [1]. The reason behind this happening is that the Voronoi cell is bounded by the proximity of other samples on the same local patch of surface while the direction of the cell is tangent to the surface. Even though the Voronoi cell of the sample point extends perpendicularly away from the surface, the sample point stops to be the closest surface point and samples on the some other patch of the surface might be closer. For this reason, the Voronoi cell of the sample point can not advance much further than the medial axis. Hence, for the densely sampled point sets, the Voronoi vertices at the two ends of the slender, long, and almost perpendicular Voronoi cell should lie near the medial axis. Therefore, two poles are roughly in the opposite direction and the pole direction from a site to its poles approximates the surface normal at that site provided the sampling condition is dense. This is one of the reasons that motivate the use of Delaunay pole sphere as an effective localization tool.

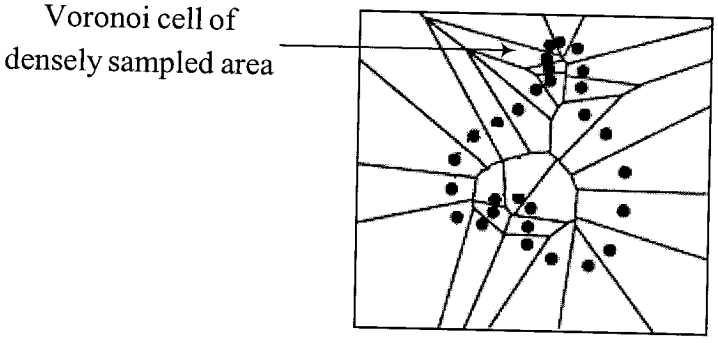

Figure 3.5: The Voronoi diagram representing the densely sampled area.

3.5.2 Performance Evaluation

The Delaunay triangulation is a global structure which is the volume representation of the surface for dense sampling. The Delaunay pole spheres are referred to as the largest

Delaunay spheres on each side of the surface. The selection of the Delaunay pole spheres as the localization tool leads to the necessity of validating the properties of Delaunay pole sphere and comparing it with other existing geometric tools used for the same purpose. Since Delaunay triangulation is the property of a number of points, some tests have been carried out to ensure that the deviation of the Delaunay pole sphere with the change of number of sample points remains within a tolerable limit. To conduct these performance tests, three types of simulated point sets have been used which are sampled from the parametric surface representation, NURBS. NURBS has been chosen over other parametric forms because of its wide acceptability in the industries as the standard tool for the representation and design of product geometry. With different geometric representations of the surfaces as shown in Figure 3.6, the three NURBS surfaces represented by point sets is termed here as Point Set 1, Point Set 2, and Point Set 3, respectively. For these tests, each test surface is sampled uniformly and randomly using same number of points. 20,000 points have been taken as the reference data set and the numbers of points have been reduced from 100% to 10%. To compare the deviation of Delaunay pole sphere between the reference data set and the reduced data set, characteristic points of each point set have been considered. This is because the characteristic points are defined in this work as those points that represent the distinct features of any free-form surface and our localization algorithm is based on these characteristic points. The identification of characteristic points in this research work will be discussed in details in a later chapter.

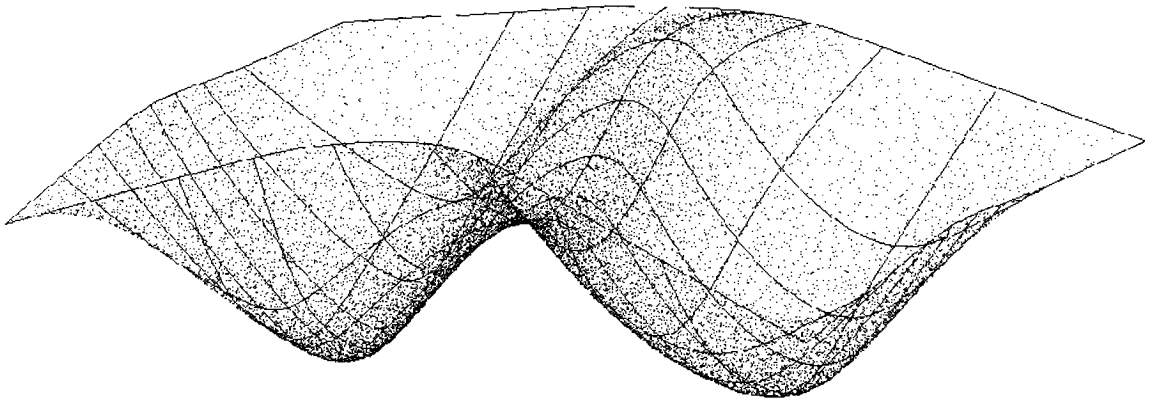

(a) Point Set 1

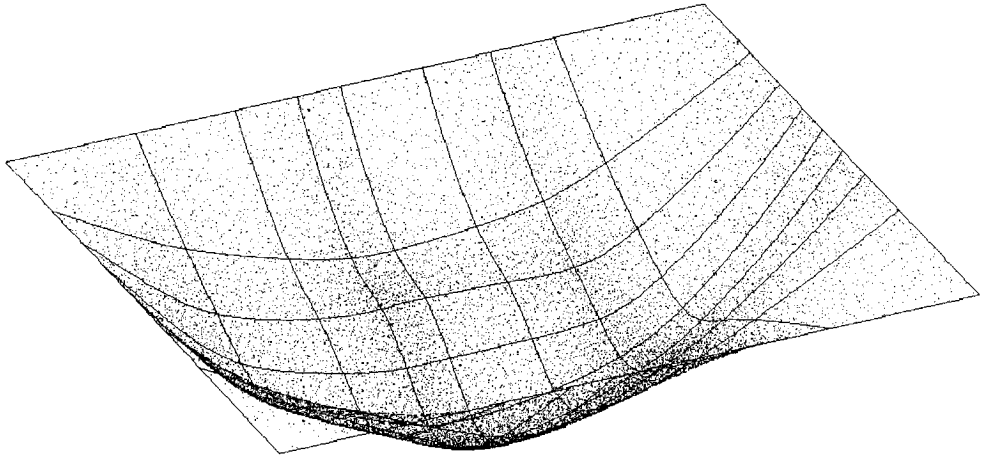

(b) Point Set 2

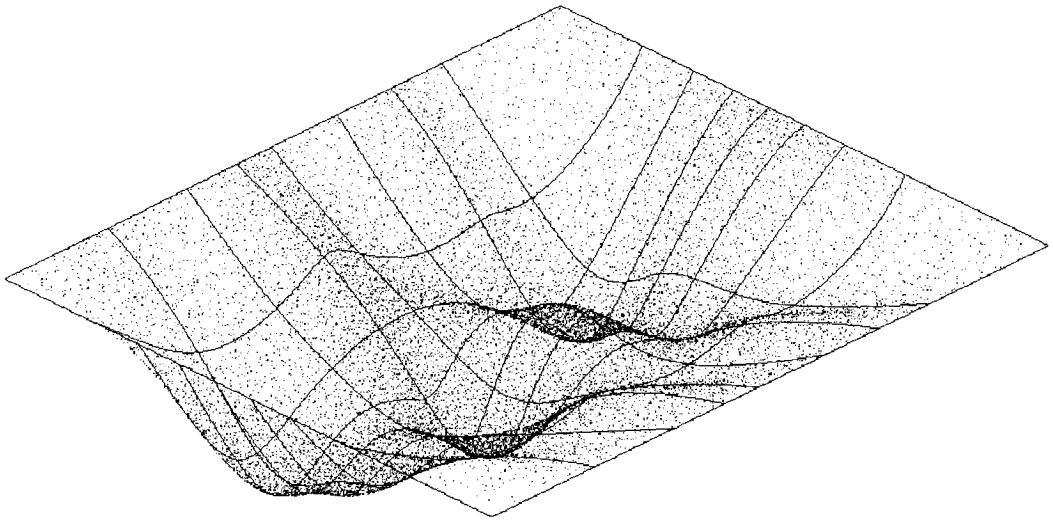

(c) Point Set 3

Figure 3.6: Simulated point sets used to examine the Delaunay pole sphere performance.

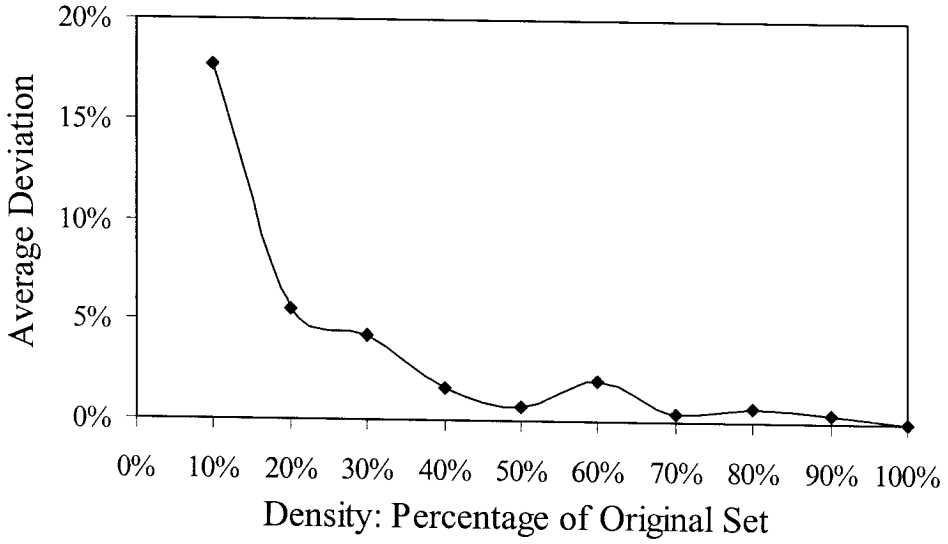

(a)

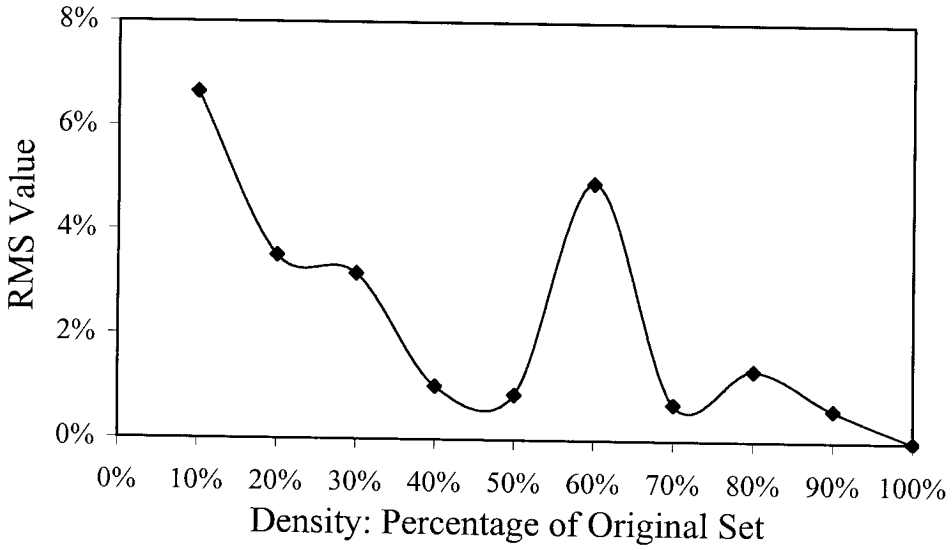

(b)

Figure 3.7: Average deviation and RMS values of Delaunay pole spheres for characteristic points in uniformly sampled Point Set 1with reduced point densities.

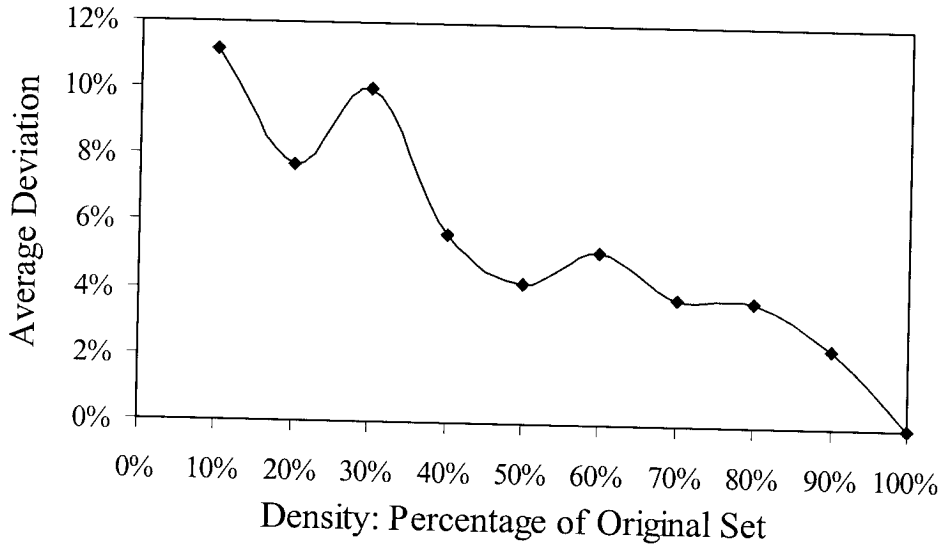

(a)

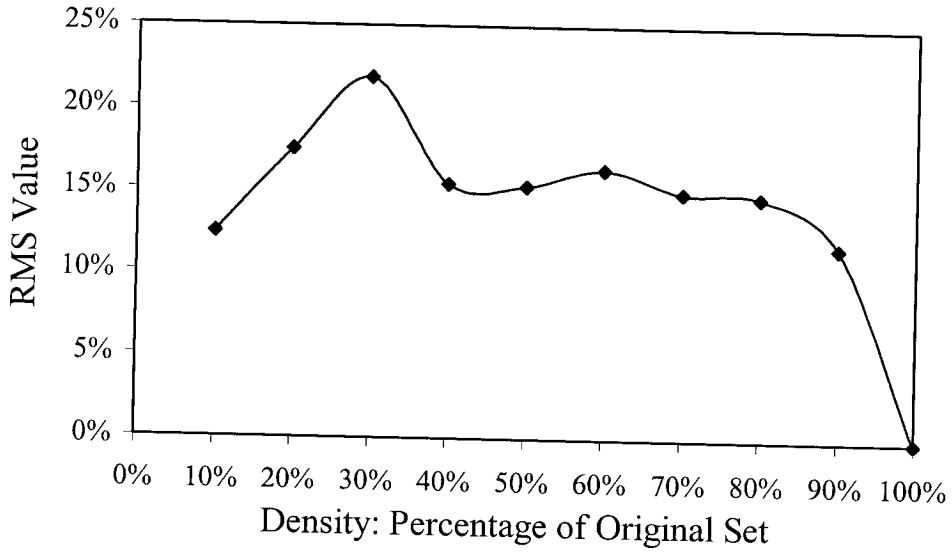

(b)

Figure 3.8: Average deviation and RMS values of Delaunay pole spheres for characteristic points in randomly sampled Point Set 1with reduced point densities.

Table 3.1: Result details of Delaunay pole sphere deviation analysis for randomly sampled Point Set 1.

	Point Number	Percentage of Original Set (%)	Density by Length	Number of Characteristic Points	Average Deviation (%)	RMS Value (%)
1	2,000	10	1.897	56	11.1	12.4
2	4,000	20	1.359	88	7.7	17.4
3	6,000	30	1.103	90	10.0	21.8
4	8,000	40	0.950	138	5.7	15.4
5	10,000	50	0.856	150	4.2	15.3
6	12,000	60	0.774	172	5.2	16.3
7	14,000	70	0.716	215	3.8	14.9
8	16,000	80	0.667	270	3.8	14.7
9	18,000	90	0.629	275	2.3	11.7
10	20,000	100	0.599	311	0.0	0.0

Figure 3.7 (a) and Figure 3.7 (b) represent the average deviation and the RMS value of Delaunay pole sphere radii, respectively using uniformly sampled Point Set 1. It has been shown that the maximum average deviation is less than 18% and the maximum RMS value is less than 7%. It has also been presented that when the difference between the point numbers of reference point set and the reduced point set lessens, generally the average deviation also decreases. Similar result using randomly sampled Point Set 1is depicted in Figure 3.8. Table 3.1 shows the detailed test result illustrating number of points, number of characteristics points, average density of point set, average deviation, and the RMS value of the reduced point sets using the randomly sampled Point Set 1. In this test case, it has been shown that the maximum average deviation is 11.1% and the maximum RMS value is 12.4% where the average deviation has the trend to decrease while difference between numbers of two point sets becomes less.

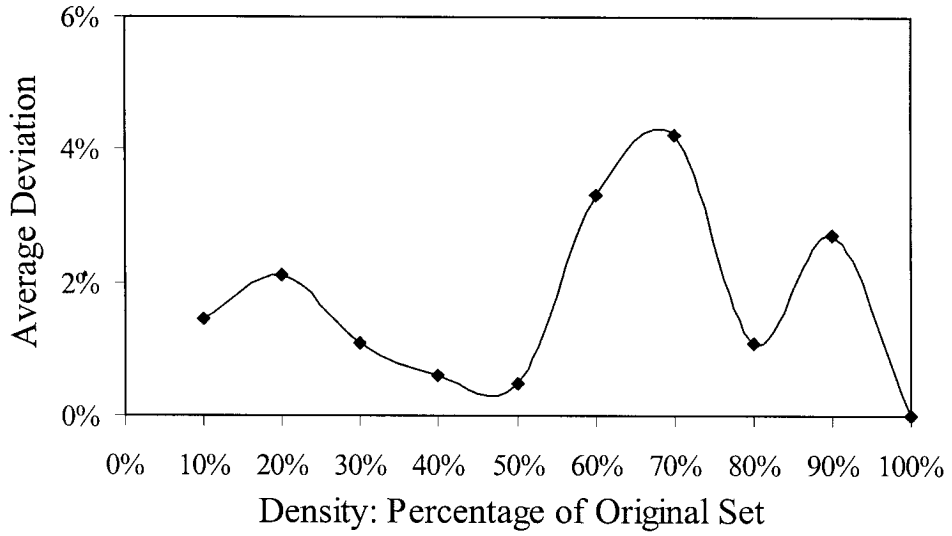

(a)

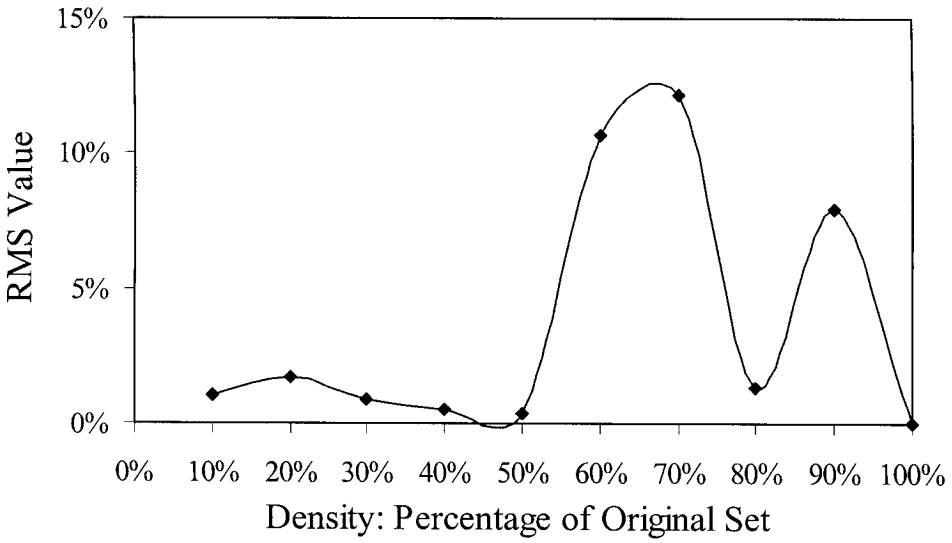

(b)

Figure 3.9: Average deviation and RMS values of Delaunay pole spheres for characteristic points in uniformly sampled Point Set 2 with reduced point densities.

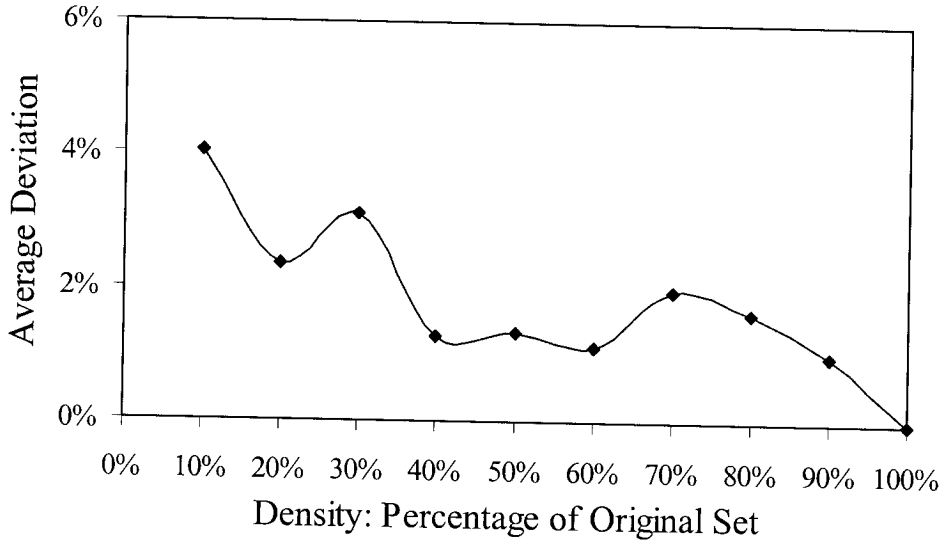

(a)

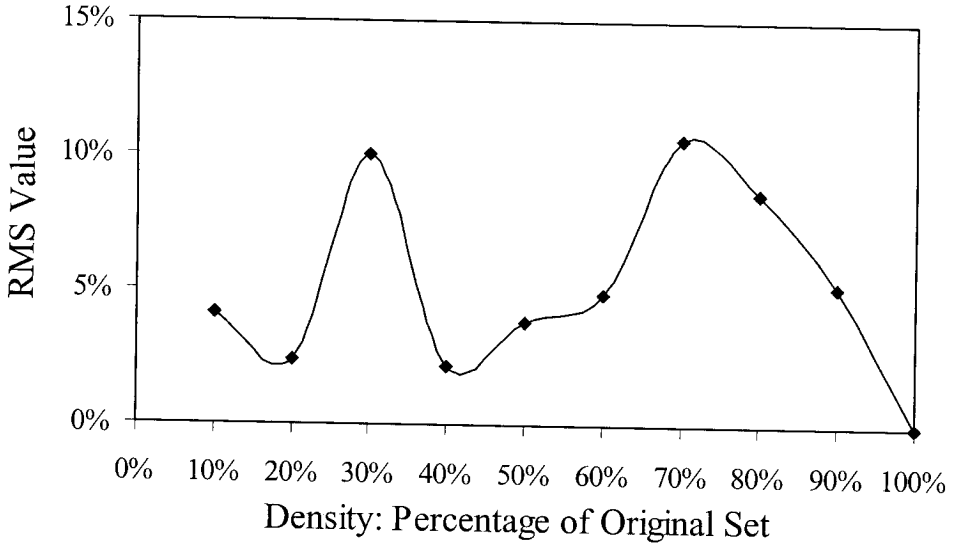

(b)

Figure 3.10: Average deviation and RMS values of Delaunay pole spheres for characteristic points in randomly sampled Point Set 2 with reduced point densities.

Table 3.2: Result details of Delaunay pole sphere deviation analysis for randomly sampled Point Set 2.

	Point Number	Percentage of Original Set (%)	Density by Length	Number of Characteristic Points	Average Deviation (%)	RMS Value (%)
1	2,000	10	1.870	27	4.1	4.1
2	4,000	20	1.303	54	2.4	2.4
3	6,000	30	1.050	53	3.1	10.0
4	8,000	40	0.904	79	1.3	2.1
5	10,000	50	0.812	123	1.3	3.8
6	12,000	60	0.737	154	1.1	4.9
7	14,000	70	0.683	200	2.0	10.6
8	16,000	80	0.636	251	1.6	8.6
9	18,000	90	0.602	290	1.0	5.2
10	20,000	100	0.569	312	0.0	0.0

The average deviation and the RMS value of Delaunay pole spheres using uniformly sampled Point Set 2 is depicted in Figure 3.9 (a) and Figure 3.9 (b), respectively. It has been shown that the maximum average deviation is below 5%, and the maximum RMS value is less than 15%. Figure 3.10 also displays (a) the average deviation and (b) the RMS value using sampled Point Set 2, but the point sets are sampled randomly. The detailed test results using randomly sampled Point Set 2 is presented in Table 3.2. It has been shown that the maximum average deviation is 4.1% and the maximum RMS value is 10.6%.

The final test results using Point Set 3 is delineated in Figures 3.10 and 3.11, the former one employing uniformly sampled points and the later one with randomly sampled points from the test surface. The detailed test results for randomly sampled points using Point Set 3 are illustrated in Table 3.3.

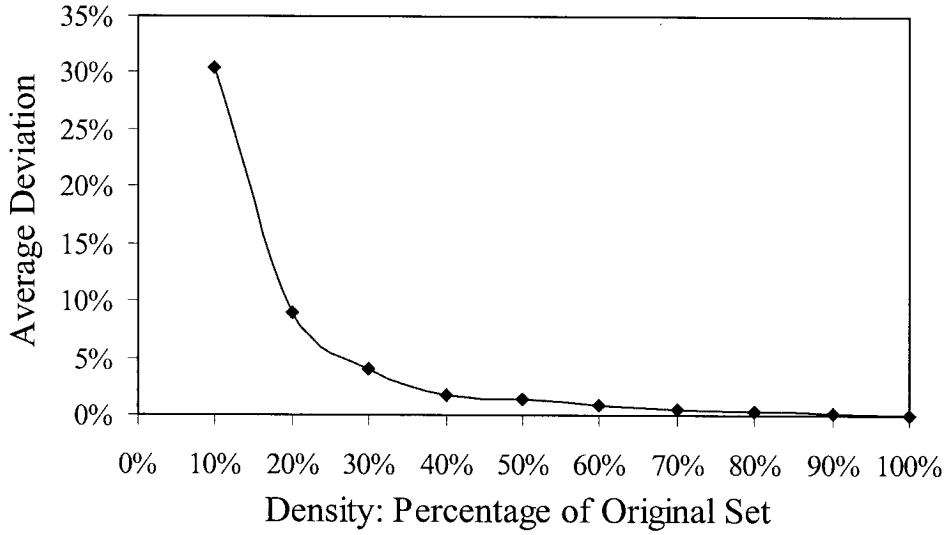

(a)

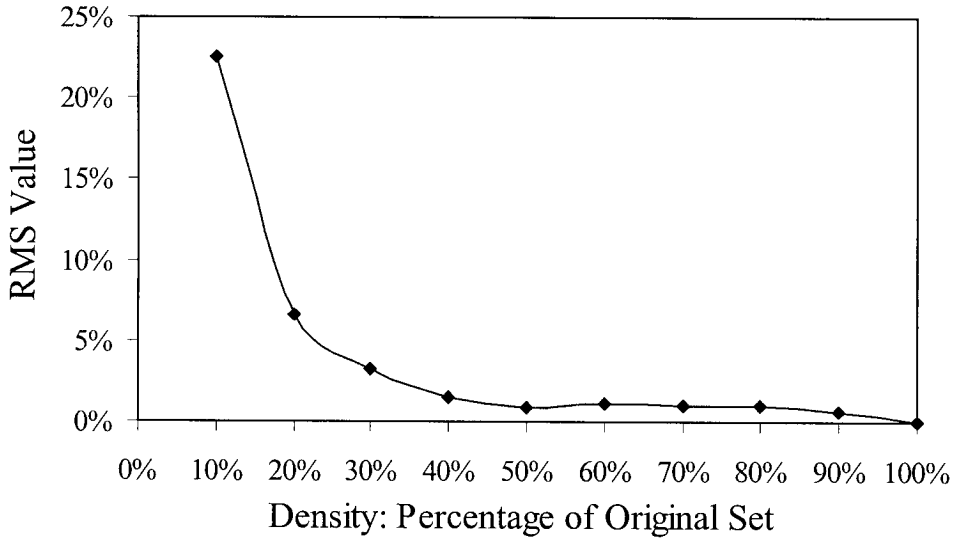

(b)

Figure 3.11: Average deviation and RMS values of Delaunay pole spheres for characteristic points in uniformly sampled Point Set 3 with reduced point densities.

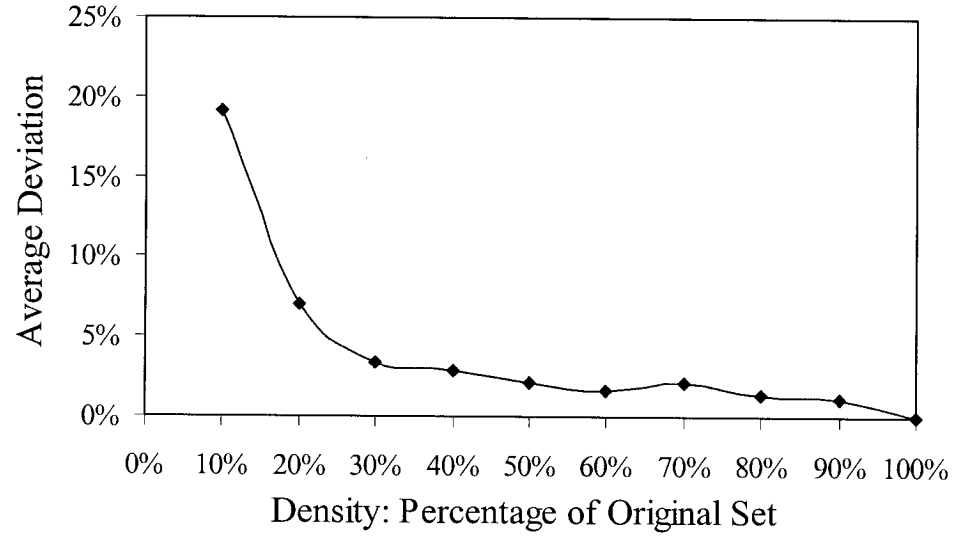

(a)

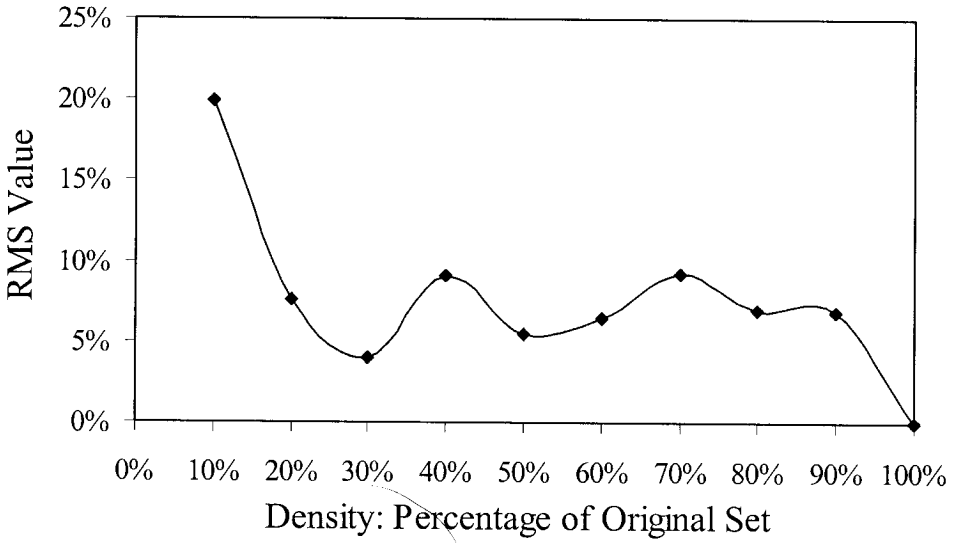

(b)

Figure 3.12: Average deviation and RMS values of Delaunay pole spheres for characteristic points in randomly sampled Point Set 3 with reduced point densities.

Table 3.3 Result details of Delaunay pole sphere deviation analysis for randomly sampled Point Set 3.

	Point Number	Percentage of Original Set (%)	Density by Length	Number of Characteristic Points	Average Deviation (%)	RMS Value (%)
1	2,000	10	1.846	45	19.0	20.0
2	4,000	20	1.322	87	7.0	7.6
3	6,000	30	1.067	117	3.3	4.0
4	8,000	40	0.926	175	2.9	9.1
5	10,000	50	0.875	180	2.1	5.5
6	12,000	60	0.753	225	1.6	6.5
7	14,000	70	0.725	294	2.1	9.3
8	16,000	80	0.646	299	1.4	7.0
9	18,000	90	0.610	329	1.2	6.9
10	20,000	100	0.582	377	0.0	0.0

The above tests involving three different types of surface representations and two different types of sampling arrangements of the point sets prove that regardless of the representation and distribution of the points, the range of average deviation for Delaunay pole sphere varies between 4% to 30%, among which most of the average deviation value lies below 15%, which propelled the selection of the Delaunay sphere as an efficient localization tool in our proposed algorithm.

3.5.3 Comparison with Intrinsic Differential Properties

The primal idea behind the correspondence search for matching problem is to identify some specific properties of sample points obtained from one surface and try to find the same properties from the other surface. Therefore, while choosing the specific properties, it should be kept in mind that those properties have to be robustly extractable. For matching two free-from surfaces, several existing work tries to utilize some intrinsic

differential properties of the surface, such as curvatures. For the surfaces with known geometric representation, the calculation of curvature is pretty straightforward. But, for the practical data sets, the estimation of curvature is still a big domain of research where many work yet to be done. It is well known that the accuracy of estimated curvature can not be guaranteed such that it can be used as an efficient feature for extracting the same feature from the other surface. This motivated not to choose any intrinsic properties of the surfaces for this work to localize two free-from surfaces. Like the performance test described in the last section, some detailed tests have been conducted using the Point Set 1, Point Set 2, and Point Set 3 to compare the average deviation of estimated Gaussian curvature with that of the Delaunay pole sphere. These tests are performed using the uniformly sample point sets for all the cases. Same number of characteristic points has been used for the calculation of the estimated Gaussian curvature and the Delaunay pole sphere.

Table 3.4 represents the detailed analysis results of Delaunay pole sphere and Gaussian curvature for uniformly sampled Point Set 1. It clearly appears from the table that, for same point set, the average deviation using Delaunay pole sphere is far below than the average deviation utilizing estimated Gaussian curvature. It shows that the maximum average deviation for estimated Gaussian curvature is 97.9%, whereas the maximum average deviation for Delaunay pole sphere is only 17.7%.

The result details of Delaunay pole sphere and Gaussian curvature analysis using uniformly sampled Point Set 2 is presented in Table 3.5 which also prove that the average deviation of Delaunay pole sphere is significantly less than that of the estimated Gaussian curvature. It has been shown that the maximum value of the Delaunay pole sphere

average deviation is 4.2% which is too low compared to 415.3%, the maximum value of the estimated Gaussian curvature average deviation.

The test results of Table 3.5 are performed using uniformly sampled Point Set 3. These results are also represented to verify that for same number of points, the average deviation of Delaunay pole sphere is distinctly less than the average deviation of the estimated Gaussian curvature.

All these results clearly prove that, for unknown geometric representations such as point cloud, the deviation of estimated curvature calculation is immense. As discussed earlier, for matching two free-form surfaces or two point sets, a specific property ought to be found from one point set which would have to be easily identified from the other set. Considering this aspect, a property with such huge average deviation clearly can not be a good choice for localization.

Table 3.4: Result details of Delaunay pole sphere and Gaussian curvature analysis for uniformly sampled Point Set 1.

	Point Number	Percentage of Original Set (%)	Density by Length	Number of Characteristic Points	Delaunay Pole Sphere		Gaussian Curvature	
					Average Deviation (%)	RMS Value (%)	Average Deviation (%)	RMS Value (%)
1	2,000	10	2.894	5	17.7	6.7	27.4	35.6
2	4,000	20	1.633	4	5.5	3.5	97.9	130.2
3	6,000	30	1.251	4	4.2	3.2	33.0	10.8
4	8,000	40	1.063	7	1.6	1.0	28.2	14.1
5	10,000	50	0.943	7	0.7	0.9	35.1	23.9
6	12,000	60	0.866	13	2.0	4.9	38.5	30.2
7	14,000	70	0.811	21	0.4	0.7	27.6	24.2
8	16,000	80	0.764	16	0.7	1.3	34.9	29.8
9	18,000	90	0.729	17	0.4	0.6	22.4	26.8
10	20,000	100	0.696	10	0.0	0.0	0.0	0.0

Table 3.5: Result details of Delaunay pole sphere and Gaussian curvature analysis for uniformly sampled Point Set 2.

	Point Number	Percentage of Original Set (%)	Density by Length	Number of Characteristic Points	Delaunay Pole Sphere		Gaussian Curvature	
					Average Deviation (%)	RMS Value (%)	Average Deviation (%)	RMS Value (%)
1	2,000	10	2.684	4	1.5	1.0	415.3	388.6
2	4,000	20	1.533	8	2.1	1.7	83.3	25.0
3	6,000	30	1.168	6	1.1	0.9	82.0	54.9
4	8,000	40	0.990	9	0.6	0.5	78.0	77.8
5	10,000	50	0.893	9	0.5	0.3	128.1	155.9
6	12,000	60	0.820	19	3.3	10.7	119.5	137.8
7	14,000	70	0.771	27	4.2	12.2	84.1	149.8
8	16,000	80	0.731	36	1.1	1.3	118.9	193.0
9	18,000	90	0.700	42	2.7	7.9	93.5	141.5
10	20,000	100	0.668	7	0.0	0.0	0.0	0.0

Table 3.6: Result details of Delaunay pole sphere and Gaussian curvature analysis for uniformly sampled Point Set 3.

	Point Number	Percentage of Original Set (%)	Density by Length	Number of Characteristic Points	Delaunay Pole Sphere		Gaussian Curvature	
					Average Deviation (%)	RMS Value (%)	Average Deviation (%)	RMS Value (%)
1	2,000	10	2.771	22	30.4	22.6	147.1	279.1
2	4,000	20	1.637	25	8.9	6.6	109.0	293.7
3	6,000	30	1.214	31	4.0	3.2	126.3	327.8
4	8,000	40	1.028	31	1.8	1.5	160.8	303.5
5	10,000	50	0.898	31	1.3	0.9	161.4	447.3
6	12,000	60	0.837	36	0.9	1.1	90.3	206.7
7	14,000	70	0.781	37	0.5	0.9	71.7	196.8
8	16,000	80	0.738	37	0.4	1.0	43.3	111.5
9	18,000	90	0.706	38	0.3	0.6	14.3	24.7
10	20,000	100	0.675	38	0.0	0.0	0.0	0.0

On the contrary, as focused in the earlier section, in many existing literatures Delaunay pole sphere has been approximated as the medial axis which is the theoretical representation of the surface. With less average deviation between two different point sets, the radius of Delaunay pole sphere can extract the corresponding radius of Delaunay pole sphere from the other point set easily. Moreover, being the property of a point set, Delaunay triangulation only depends on the distribution and density of the points. They are also steady under any rigid body transformation (rotation and translation). Keeping all these in mind, Delaunay pole sphere has been chosen in this research work as a robust tool for the initial matching algorithm.

Chapter 4

Preprocessing Prior to Initial Matching

Data preprocessing is a concept of process performed on source data to prepare it for another processing procedure. It transforms the raw data into a format that will be more easily and effectively processed for further operation. Since the basic idea behind the three dimensional object matching for computer aided inspection system is to align two objects as closely as possible, two source datasets are of interest in the context of this thesis. Among those two, one is the design model or CAD model represented by the point cloud data which can be termed as the reference data set whereas the other one is the measurement point set obtained from the contact or non-contact measuring devices. To accomplish the accurate correspondence search, whether the two input datasets should go through a processing step before starting the proposed algorithm for localization or should be used directly as the raw datasets is a significant issue to be considered. This Chapter deals with the basic concepts pertaining to preprocessing steps before initial matching is initiated.

4.1 Preprocessing Data Set

The CAD model is usually represented by the parametric form of NURBS formulation. With known mathematical formulation, dealing with the design model is straightforward

and points can be conveniently sampled from the theoretical surface using different sampling techniques. When the sample points are sufficiently dense, those points can be treated as the true representation of the shape of the surface. In this work, the CAD surface is always sampled dense enough so that it can represent the geometry of the object properly and hence no preprocessing is performed on the raw data points obtained from the CAD surface in the proposed approach. On the other hand, the manufactured product is usually measured by the CMM machine or scanned by some scanning devices such as laser scanner from which the point sets are obtained in discrete data form. Measuring point sets from the manufactured product depends on many factors such as different types of measurement devices used, scanning direction, and scanning speed. All these factors make the nature of measurement data highly unpredictable and this data attains further interest of processing to smoothen out its fuzzy characteristics. To this end, in this work the measurement data set is considered for preprocessing while needed.

4.2 Method of Preprocessing

The goal of the localization is to find the relative position and orientation of one point set obtained from the measurement data with respect to the point set obtained from the CAD model. Given the two input data point sets from measurement data and CAD model, the proposed method is started by preprocessing the measurement data (if needed) according to the following steps.

Point Spacing Calculation: At first, the average point spacing of the measurement data set, ρ_D and the average point spacing of the CAD model, ρ_M have been calculated.

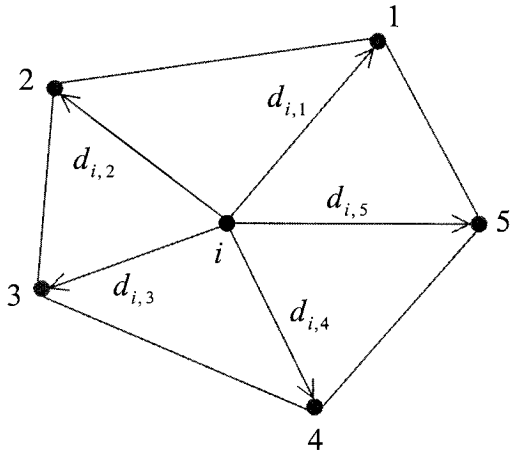

Figure 4.1: Depiction of neighboring points of the i th point.

The point spacing calculation performed in this work is based on the distance criterion. The point spacing of the ith point of data set is defined in this work as given by

$$\rho_i = \frac{\sum_{j=1}^{N_i} d_{i,j}}{N_i} \tag{4.1}$$

where N_i is total number of local neighboring points of the ith point and $d_{i,j}$ is the distance between the ith point and its jth neighboring point. Figure 4.1 shows the respective distance between the ith point and the five neighboring points of its local mesh. The average point spacing of each point set is calculated by taking average of the point spacing of all the points of that set. Triangular mesh has been constructed using the Delaunay cell clustering method proposed by OuYang and Feng [44]. After the construction of the closed local mesh for each point i, surrounding points of the mesh for that point have been considered as its neighboring points for purpose of point spacing calculation.

Point Spacing Comparison: After the average point spacing for both the measurement point set and the CAD model point set has been computed, a comparison between the average point spacing is made. If the CAD model set is denser than the measurement point set that means if the average point spacing of the CAD model is smaller than that of the measurement data, i.e., $\rho_M < \rho_D$, it is considered as the stable situation for performing the localization. In this case, no processing on any of the data set is performed that means the source data set is kept as it is. On the other hand, if the measurement point is denser, this point set has to be processed to a suitable form. No processing is performed on the CAD model point set as usual.

Processing Based on Point Spacing: The measurement point set with higher density is processed such that its density becomes lower. Since the new invariant property, Delaunay pole sphere, used for initial matching in this work is derived from the computational geometric technique, Delaunay triangulation which is a property of point density, the measurement points are reduced in such a way that the average point spacing of the CAD model and the measurement point becomes similar. For making the point spacing alike, measurement points are thrown out from the measurement point cloud in a uniform manner so that it does not affect the distribution of the point set and the representation of the surface. A user defined parameter; the density reduced factor u, is introduced for reducing the density to a desired level. As the motivation behind this preprocessing step is to make the density of both point sets similar, the density reduced factor u is assigned to be 1 for preprocessing. As an example, to reduce the density of the measurement point set to half of the density of the CAD model point set, the density reduced factor u will be 2. Depending on the noise of the data set, this value of the

density reduced factor might vary to smoothen out the noise effect, which will be shown elaborately in a subsequent chapter.

4.3 Justification of Preprocessing

Two main reasons play the important role for considering the measurement point set to go through the steps of checking the density and preprocessing the set depending on the density requirement, instead of using the source data sets directly for initial matching. The availability of correspondent points and the deviation due to the noise are the two prime reasons for introducing the concept of preprocessing.

4.3.1 Availability of Correspondence

For the correspondence search in localization, the correspondent points of the measurement data have to be extracted from the CAD model with the help of some specific properties of the measurement points. While using the efficient property, the Delaunay pole sphere, of some characteristic points of the measurement data set to find out the correspondent points from the CAD model, points with the similar value of that property must have to be present in the CAD model. If the measurement point set is denser than the CAD model point, the size of Delaunay pole sphere of the measurement data might be too small compared to the Delaunay pole sphere of the CAD model set, which might create the uncertainties of finding the corresponding point from the CAD model with same or within tolerance Delaunay pole sphere size. If those corresponding points do not exist in the CAD model data set, the reference measurement points will try to do the best possible search from the CAD model sets with increased tolerance. Hence,

the characteristic measurement points used for the correspondence search might end up finding the wrong correspondent points from the CAD model. There is a possibility for these wrong corresponding points to be found in a position far away from the correct position. This will end up with wrong initial transformation information, and the localization of the CAD model and measurement point will not be obtained. On the other hand, if the measurement point set is less dense than the CAD model point, the Delaunay pole sphere size of the measurement point might be bigger than that of the CAD model point, which still can pick up the corresponding point from CAD model within the tolerable Delaunay pole sphere size.

To avoid this situation, we try to make sure that measurement point density is always less than the CAD model point density. Hence, the comparison of density between the CAD model points and the measurement points has been performed before starting the initial matching algorithm, and the excess measurement points are thrown away in a uniform manner for reducing the density of the measurement data set.

4.3.2 Deviation Due to Measurement Error and Noise

For measuring the manufactured products, contact and non-contact devices are used among which the contact device, CMM is the high accuracy device whereas the non-contact device, laser scanner is a high speed device but not as accurate. The measurement data contains measurement error whose properties depend on both the distance from the surface to the viewpoint and the relative orientation of the surface to the viewing direction. As a result, the properties of measurement error are different for each point. The data obtained from laser scanner devices always have noise which is smaller than the

tolerance of the used instruments. Noise in the measurement process can be considered as any difference in the data that is not directly attributable to the surface being measured. Any change in the test environment can cause noise in the measurement. It affects the accuracy and the repeatability of the measurement and the noisy data do not allow a correct interpretation of the object details.

To examine the behavior of noise on the point sets, some tests have been conducted using three simulated point sets which are sampled from the surfaces with different representation of NURBS formulation as mentioned in Chapter 3. Delaunay pole sphere, the invariant property, used for initial matching in the proposed approach has been used in this test.

Each test surface has been sampled uniformly and Gaussian noise (10%) has been added to each point along its normal direction. The point density has been reduced with respect to a reference density and the nature of the average deviation of the Delaunay pole sphere has been examined for these noisy data. Figure 4.2 (a) depicts the average deviation and Figure 4.2 (b) displays the RMS value of the Delaunay pole sphere radii, respectively, using the characteristic points with varying densities for Point Set 1. We added 10% noise with the measurement sampled data for both cases. Similar results have been shown in Figures 4.3 and 4.4 for Point Set 2 and Point Set 3, respectively.

All these test results depict the trend for deviation of Delaunay pole sphere for the noisy data set. It clearly shows that reducing the density reduces the average deviation of the Delaunay pole sphere radii.

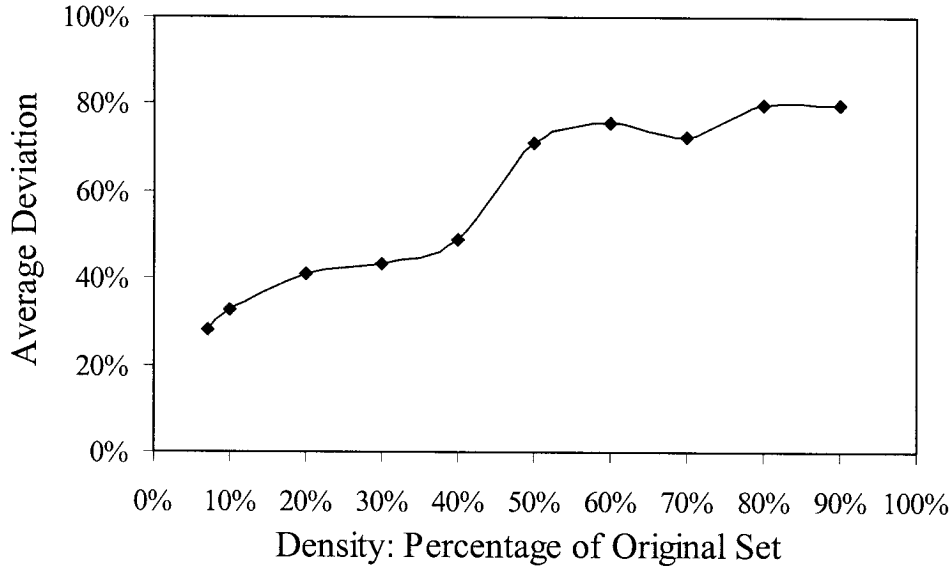

(a)

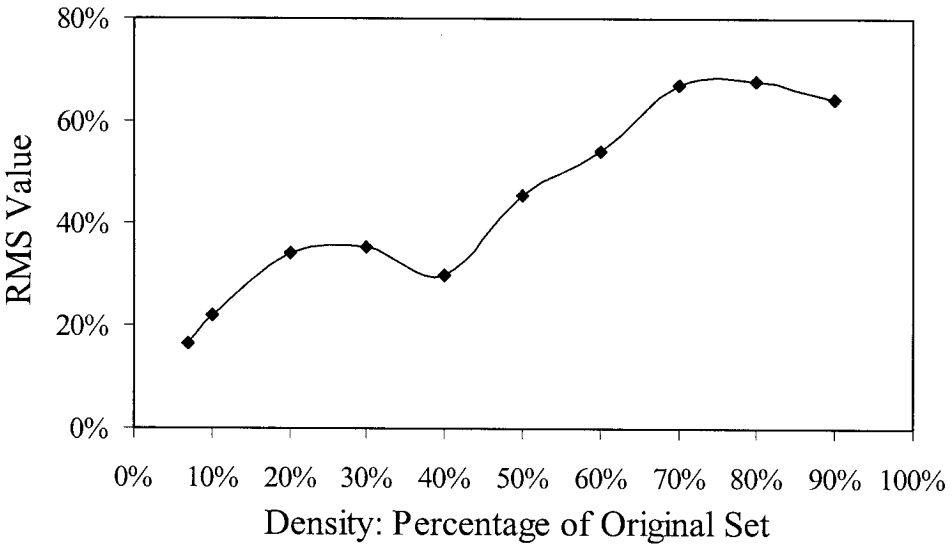

(b)

Figure 4.2: Average deviation and RMS values of Delaunay pole spheres for characteristic points in uniformly sampled Point Set 1 with 10% noise and reduced densities.

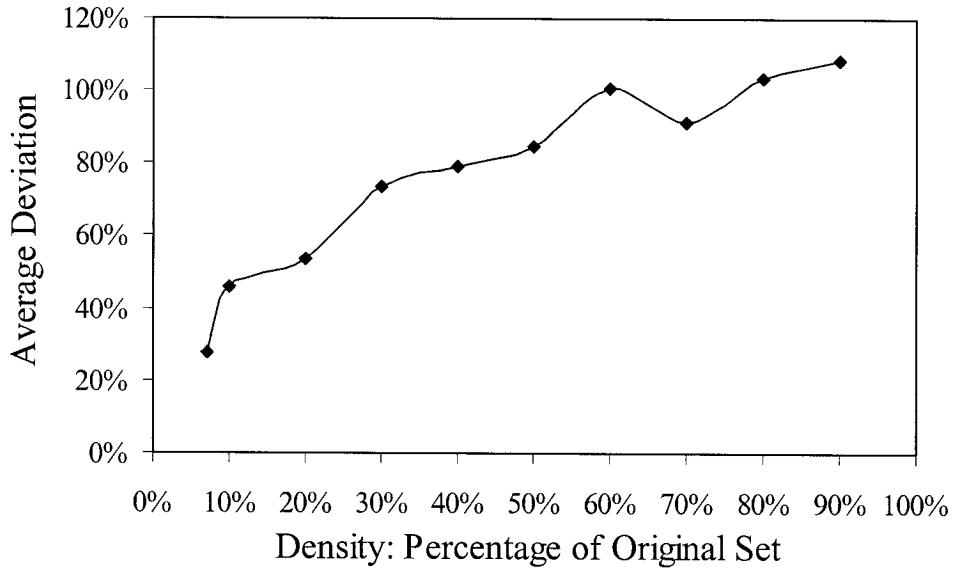

(a)

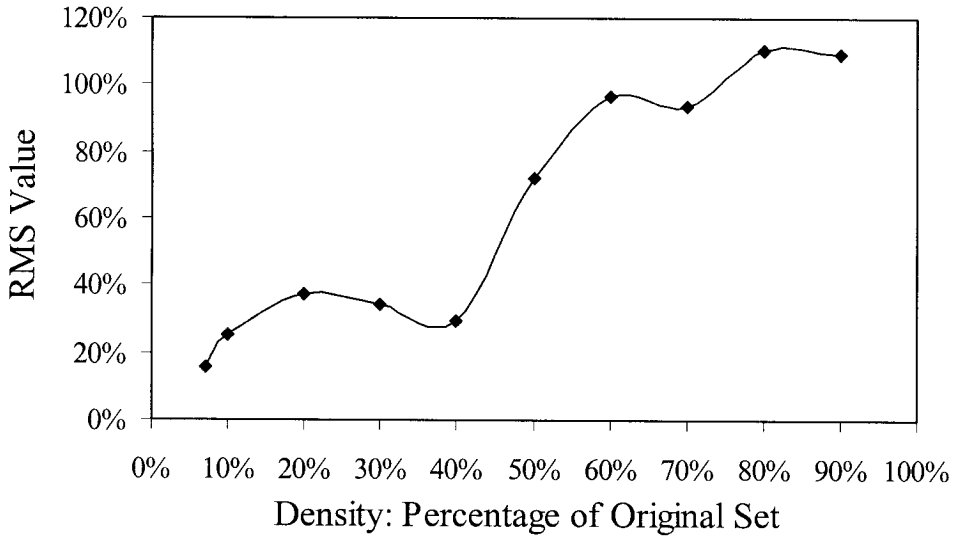

(b)

Figure 4.3: Average deviation and RMS values of Delaunay pole spheres for characteristic points in uniformly sampled Point Set 2 with 10% noise and reduced densities.

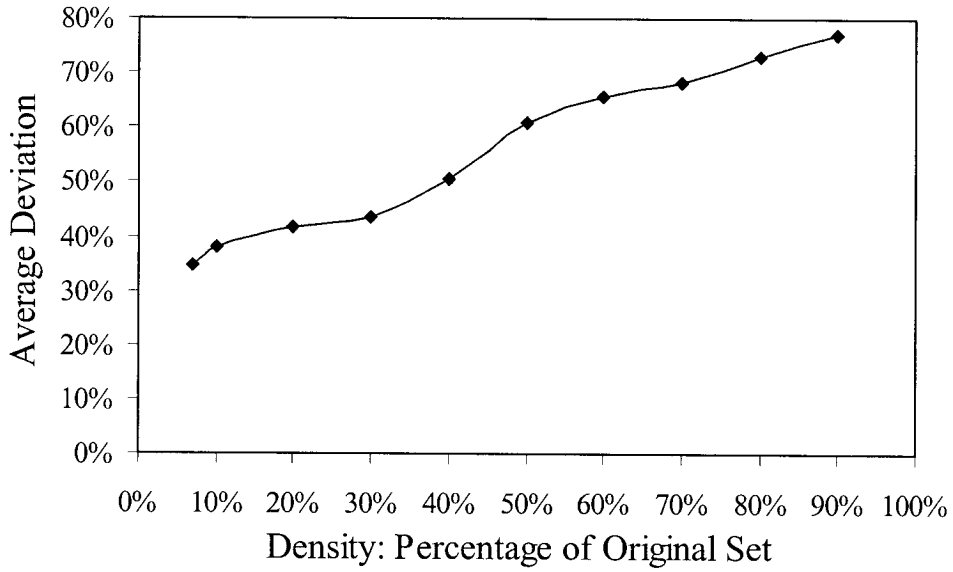

(a)

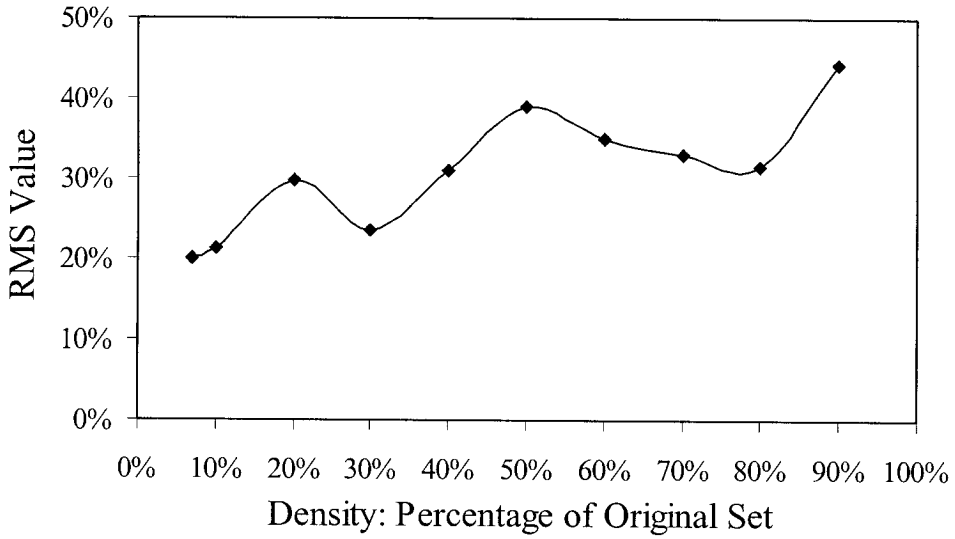

(b)

Figure 4.4: Average deviation and RMS values of Delaunay pole spheres for characteristic points in uniformly sampled Point Set 3 with 10% noise and reduced densities.

Since the vertices of the Delaunay tetrahedron forms the Delaunay sphere, in case of noisy data, the change in the x, y, z coordinates of the densely sampled measurement points has more probability of producing a different Delaunay sphere with higher deviation with respect to the original one. Reducing the point density has a very high possibility of smoothing out the noise effect on the size of the Delaunay sphere.

To this end, when the measurement point set is denser than the CAD model point set, preprocessing has been performed on the measurement data set by reducing its density. Due to the irregular nature of the noise, it is tedious to estimate the optimum level of the density reduction. We consider the threshold for density reduction such that average point spacing of the measurement points is of approximately equal to the average point spacing of the CAD model points. The proposed initial matching algorithm incorporating preprocessed data set will be discussed next.

Chapter 5

Initial Matching Algorithm

This chapter investigates the problem of initial matching of free-from objects in the context of automatic inspection system to establish correspondences between the point cloud data obtained from those objects while no *a priori* information of transformation or correspondence is available. The goal of inspection is to check a given product for identifying manufacturing errors and to visualize and classify the deviations. An automated inspection system can be investigated as follows: a product is manufactured according to the design specified in its CAD model. The manufactured product is measured with different measuring devices resulting 3D point cloud data from the surface of this product. Thereby, the CAD model describes the ideal shape of the object and will be available in a coordinate system that is different to that of the 3D data point set obtained from the measuring devices. To this end, it is of interest to find the optimal transformation parameters (translation and rotation) that aligns or localizes the measurement point cloud to the CAD model. The correspondence information between the CAD model and the point cloud is the key factor in finding the best transformation to perform the localization between two point sets.

Based on an effective computational geometric tool which is invariant under any rigid body transformations, in this chapter, we propose a robust estimation approach in estimating transformation parameters to achieve free-form object matching without the availability of initial correspondence information.

5.1 Procedure of the Algorithm

In this section, the proposed robust initial matching approach is introduced in a sequential manner. For initiating the algorithm, as explained in the previous chapter, the measurement data set is preprocessed if the average density of the CAD model set, ρ_M is greater than the average density of measurement point set, ρ_D. After preprocessing the measurement data while needed, this proposed approach comprises the following steps.

5.1.1 Delaunay Triangulation and Mesh Construction

The proposed initial matching algorithm is initiated by the Delaunay triangulation of the input point sets. The point set sampled from the CAD model and the point set obtained from the preprocessed measurement data are considered as the input point sets for the proposed algorithm. Next, triangular mesh is constructed using the Delaunay cell clustering method reported in [44] in order to obtain the Delaunay pole sphere, an efficient tool to accomplish localization. As discussed in the preceding chapter, for each point, its local Delaunay triangular mesh is calculated maintaining all local triangular mesh directions constant and all the Delaunay spheres of each point are divided into two groups by using this constructed local mesh.

Based on an effective computational geometric tool which is invariant under any rigid body transformations, in this chapter, we propose a robust estimation approach in estimating transformation parameters to achieve free-form object matching without the availability of initial correspondence information.

5.1 Procedure of the Algorithm

In this section, the proposed robust initial matching approach is introduced in a sequential manner. For initiating the algorithm, as explained in the previous chapter, the measurement data set is preprocessed if the average density of the CAD model set, ρ_M is greater than the average density of measurement point set, ρ_D. After preprocessing the measurement data while needed, this proposed approach comprises the following steps.

5.1.1 Delaunay Triangulation and Mesh Construction

The proposed initial matching algorithm is initiated by the Delaunay triangulation of the input point sets. The point set sampled from the CAD model and the point set obtained from the preprocessed measurement data are considered as the input point sets for the proposed algorithm. Next, triangular mesh is constructed using the Delaunay cell clustering method reported in [44] in order to obtain the Delaunay pole sphere, an efficient tool to accomplish localization. As discussed in the preceding chapter, for each point, its local Delaunay triangular mesh is calculated maintaining all local triangular mesh directions constant and all the Delaunay spheres of each point are divided into two groups by using this constructed local mesh.

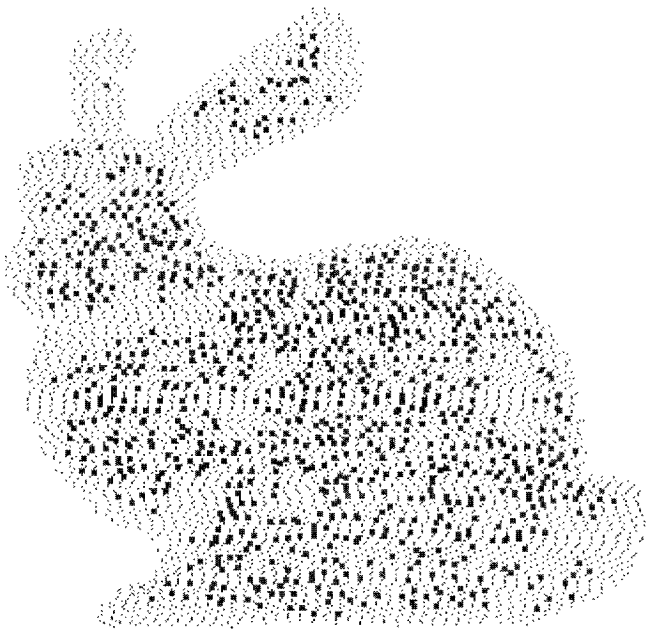

Figure 5.1: Identified characteristic points of one-sided view of the Stanford Bunny.

Hereinafter, these two groups are considered to be in the two sides, termed as inside and outside respectively, along the sampled curve/surface. From each side, the sphere of maximum size is chosen as the Delaunay pole sphere. In this work, the Delaunay pole spheres will be utilized to establish correspondence search.

5.1.2 Characteristic Points Identification

Since the characteristic points are the points with distinct features of the data set, at first the characteristic points of the measurement point set are calculated to establish an optimal correspondent relationship between the CAD model and the measurement data set. After constructing the local mesh for each point of the measurement data set, points which follow certain conditions are treated as the feature points or the characteristic

points of the data set. Two fundamental criterions for being the characteristic points are mentioned below. Hence, a point is considered as the characteristic point if

1. each neighboring point of its closed local mesh can form closed local mesh by itself, and
2. Delaunay pole sphere of this point on any side (inside or outside) is less than that of any other local neighboring points on the same side.

Figure 5.1 represents the characteristic points computed from one of the practical data set, the Stanford Bunny [63], used to test the proposed algorithm which will be shown in the next chapter. In this test, the points obtained by scanning one-sided view of the bunny are considered as the measurement point set.

5.1.3 Ill-Conditioned Points Removal

Objects often have regions that are not easily accessible to scanning and so remain undersampled or unsampled. Some points in undersampled regions are needed to be removed from the measurement data set before further processing since the points in these regions might affect the effectiveness of the correspondence search. After constructing the triangular mesh for the measurement data set, points which construct closed local mesh are considered as the stable points and are used for further processing. If a point does not have a closed local mesh, it means either the point is on the boundary of the surface or in a hole. This point is referred to as an ill-conditioned point and is not considered anymore. These points were not evaluated due to the fact that the Delaunay spheres had the potential of generating an infinite solution in these regions.

5.1.4 Reference Triangle Selection

The proposed algorithm reduces the correspondence search drastically by choosing three points with specific properties from the measurement data and extracting three corresponding points from the CAD model having the same properties. After identifying the characteristic points as well as removing the ill-conditioned points from measurement

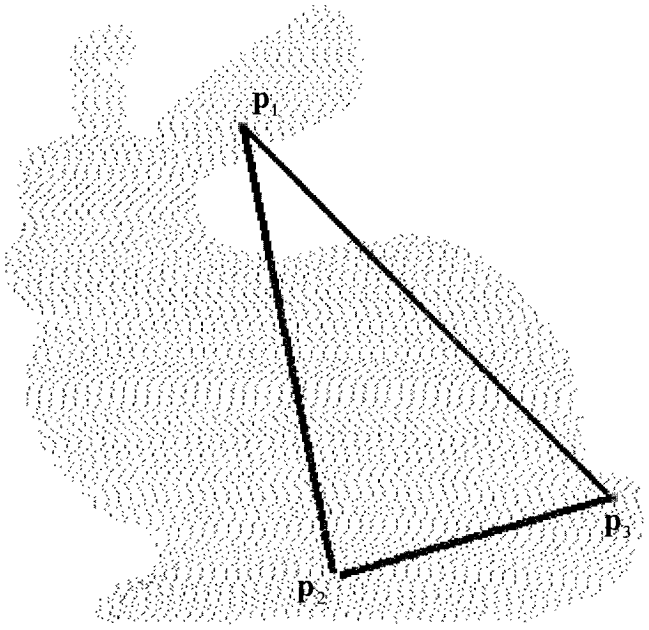

Figure 5.2: Selected reference triangle of one-sided view of the Stanford Bunny.

data set, a reference triangle has been selected from those characteristic points to obtain a good initial estimate of transformation. To this end, minimum Delaunay pole spheres are calculated for all the characteristics points of the measurement data set on each side of the curve/surface. The computed minimum Delaunay pole sphere on one side of the surface is taken as the first point and the computed minimum Delaunay pole sphere on the other side is taken as the second point of the triangle. The third point of the triangle is

chosen such that the first two selected points construct the maximum triangular area with the third point. The reason behind selecting the third point in this manner is to cover the region of the whole point set as much as possible.

Figure 5.2 depicts the selected reference triangle on the practical test data, Stanford Bunny. In this figure, $\mathbf{p}_1$ and $\mathbf{p}_2$ are the points of minimum Delaunay pole spheres on both side, respectively, and $\mathbf{p}_3$ is the point which constructs the maximum triangular area with $\mathbf{p}_1$ and $\mathbf{p}_2$.

5.1.5 Correspondent Triangle Search

Once a reference triangle is selected from the measurement data set, the correspondent triangle has to be extracted from the CAD model point cloud satisfying some predetermined constraints. Since identifying the correct correspondent triangle provides the correct transformation information, these constraints have to be chosen in an efficient manner. Two criterions have been used in this work for searching the correspondent triangle of the reference triangle; among those two, the first one is the Delaunay pole sphere criterion whereas the second one is the triangular edge criterion. How these criterions are imposed are described next.

Criterion Based on Delaunay Pole Sphere

Based on the Delaunay pole sphere radii of the three vertices of the reference triangle, a bunch of corresponding points for each vertex is obtained from the CAD model. The minimum Delaunay pole sphere radius of the Delaunay pole spheres on both sides of each vertex of the reference triangle is used as the search criterion. For each vertex, the

entire CAD model set is searched to find out all the possible corresponding points whose Delaunay pole sphere radii are within a certain tolerance of the reference Delaunay pole sphere radius.

Two Delaunay pole sphere radii pertaining to both sides of ith vertex of the reference triangle as r_1^i and r_2^i, $\{i = 1, 2, 3\}$, is denoted respectively. The minimum Delaunay pole sphere radius between r_1^i and r_2^i is denoted by $r_{\min}^i$. For each vertex, $\mathbf{p}_i$ of the reference triangle, the entire CAD model point set M of N_m points, $\{\mathbf{m}_1, \mathbf{m}_2, \ldots, \mathbf{m}_{N_m}\}$ is searched in such a way that it satisfies the following criterion

$$w_k^j = r_{\min}^i \pm \gamma^i \qquad \forall \mathbf{m}_j \in M,\ \{k = 1, 2\} \text{ and } \{j = 1, 2, \ldots, N_m\} \tag{5.1}$$

where w_1^j and w_2^j are the Delaunay pole sphere radii pertaining to both sides of the jth point of the set M, respectively, and γ^i is the user-defined tolerance value for corresponding search of ith vertex of the reference triangle. From (5.1), it can be seen that a number of points from the CAD model can be obtained corresponding to each vertex of the reference triangle.

Criterion Based on Triangular Edge

After a group of corresponding points for each vertex of the reference triangle is identified satisfying the above criterion, the edge of the reference triangle criterion is used to obtain the corresponding triangle from the CAD model. To achieve this purpose, the length of each triangular edge of the reference triangle is computed and is used as the reference length to search the corresponding triangular edges from the CAD model within a user-defined tolerance.

For each vertex $\mathbf{p}_i, \{i = 1, 2, 3\}$ of the reference triangle, three corresponding points $\{\mathbf{q}_1, \mathbf{q}_2, \mathbf{q}_3\}$ are selected from those identified corresponding points to construct the corresponding triangle from the CAD model in such a way that it satisfies the following Euclidean distance constrains simultaneously

$$\left|\left(\|\mathbf{p}_1 - \mathbf{p}_2\| - \|\mathbf{q}_1 - \mathbf{q}_2\|\right)\right| \leq \zeta^1 \tag{5.2}$$

$$\left|\left(\|\mathbf{p}_2 - \mathbf{p}_3\| - \|\mathbf{q}_2 - \mathbf{q}_3\|\right)\right| \leq \zeta^2 \tag{5.3}$$

$$\left|\left(\|\mathbf{p}_3 - \mathbf{p}_1\| - \|\mathbf{q}_3 - \mathbf{q}_1\|\right)\right| \leq \zeta^3 \tag{5.4}$$

where $\zeta^i, \{i = 1, 2, 3\}$ is the user-defined tolerance for corresponding search of ith edge of the reference triangle. Depending on the user-defined tolerance ζ^i, the number of corresponding triangles obtained from the CAD model might vary from one to many.

Since the above two criterions for correspondence search depend on the user-defined parameters, with large tolerance values, the number of corresponding triangles might be too many resulting high computational time. If the number of corresponding triangles is large, to avoid this situation, we consider reducing the number of corresponding triangles obtained from the CAD model taking resort to the following two aspects.

1. Since the first two vertices of the reference triangle were selected such that the minimum Delaunay pole spheres of both vertices were on the opposite side of each other, the first two vertices from the correspondent triangles are also checked to find whether the tolerance satisfied Delaunay pole spheres of these two vertices are on the opposite side or not. If those Delaunay pole spheres are on the same side, the corresponding triangle is not considered anymore.

2. Among all the corresponding triangles, we try to cluster the triangles in groups such that any triangle of a particular group will represent the whole group. For clustering a number of corresponding triangles in a group, we utilize the angle between two triangular planes. If the angles between the planes of the triangles are within a small threshold, they are considered as belonging to the same group. After this clustering, we pick one triangle from each group as they will provide the similar initial estimate of transformation information for initial matching.

Hence the number of corresponding triangles is reduced to an acceptable limit. However, we are motivated to find out the best correspondent triangle from the CAD model corresponding to the reference triangle of the measurement data to obtain the best initial correspondence information which is discussed next.

5.1.6 Optimal Triangle Identification

Among the corresponding triangles obtained from the CAD model, the optimal triangle has to be identified for estimating good initial transformation information. Since the idea behind the initial matching is to get an optimal initial estimate of transformation, the Delaunay pole sphere is used to obtain the optimal triangle from the corresponding triangles of the CAD model. Being a specific property of the point set, Delaunay pole sphere provides the distinct feature information for the two point sets to be matched. Moreover, since the Delaunay pole sphere for any point is constructed using three more neighboring points, Delaunay pole sphere of each point provide more information of surrounding points rather than only that point taken into consideration To obtain the optimal triangle, if distance between the corresponding points were used rather than the

Delaunay pole sphere size difference between those point sets, there would have been a higher probability of obtaining local minimum solution. Specially, if the number of points is too low, using distance between points might provide worse solution. Considering all these aspects, Delaunay pole sphere was chosen over the distance for obtaining the optimal triangle which will provide a good initial estimate of transformation.

Identification of the optimal triangle starts by computing the transformation matrix between the reference triangle and each corresponding triangle. Using this computed transformation information for every single corresponding triangle; all the characteristic points from the measurement data set are transformed to align with the CAD model. After transforming the characteristic points of the measurement data, we compute the points from the CAD model closest to each transformed characteristic point. For increasing the computation speed of closest point calculation, we divide the region into grids by constructing a tree-data structure, Octree. Therefore, the closest point can be calculated from a small region rather than searching all points in the set. We now have two point sets with equal number of points for each corresponding triangle: one from the measurement data and the other from the CAD model. Next, for each corresponding triangle, sum of the differences between minimum Delaunay pole sphere radii of each closest point pair of those two sets is evaluated. The correspondent triangle which gives the minimum value of all the sums is considered in this work as the optimal triangle for initial matching. Figure 5.3 depicts the identification of the optimal triangle represented by three vertices $\mathbf{q}_1, \mathbf{q}_2,$ and $\mathbf{q}_3,$ respectively, from the whole view of the Stanford Bunny, corresponding to the reference triangle represented by three vertices $\mathbf{p}_1, \mathbf{p}_2,$ and $\mathbf{p}_3,$ respectively as shown in Figure 5.2.

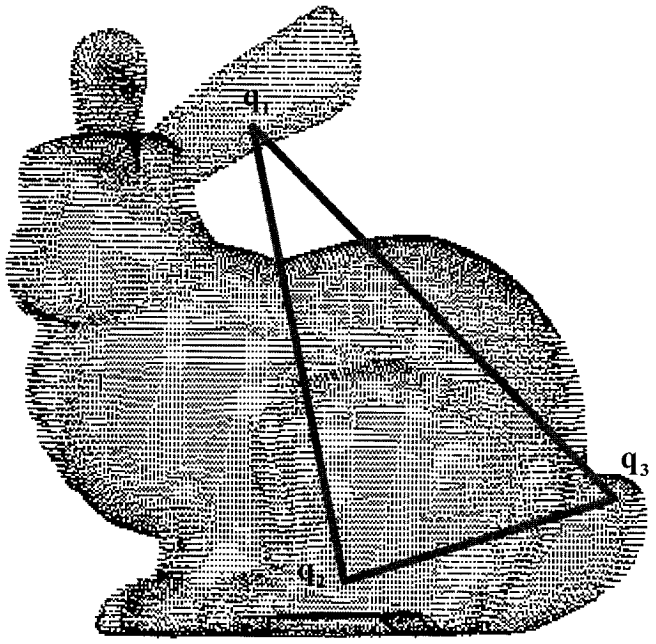

Figure 5.3: Optimal triangle obtained from the Stanford Bunny.

5.2 Implementation of the Algorithm

For implementing the proposed initial matching approach, the ICP algorithm is incorporated which utilizes the required initial transformation parameters obtained from the initial matching algorithm and localizes the CAD model and the measurement data for inspecting the manufacturing error. To evaluate the performance of the proposed algorithm, the performance index used in this work is the MSE between the localized measurement point set and its corresponding points from the CAD model set. Another factor for evaluating the performance is to review two data sets visually whether the CAD model point set and the transformed measurement data set localizes efficiently.

In practical situation, measurement data is obtained in the form of discrete data and the data set can be perturbed by the measurement error or noise. While dealing with

this noisy data whose behavior is quite unpredictable, the proposed algorithm might not work properly. Considering this aspect, an approach has been implemented to smoothen out the detrimental effect of the perturbed data.

The localization technique is started with two input point sets: the CAD model and the preprocessed measurement data. For preprocessing, the density of the measurement data is reduced to have the similar density of the CAD model using the density reduced factor $u = 1$ as discussed in Chapter 4. The method for implementing the localization algorithm can be described as follows:

1. ***Increasing Tolerance:*** Two user-defined tolerance values are set to search the optimal correspondent triangle in the initial matching algorithm as discussed in Section 5.1. If no correspondent triangle is available, the tolerance values are increased within an acceptable limit to obtain the correspondent triangle. With the increased tolerance value, the initial matching algorithm might end up finding some corresponding triangles or might not obtain any triangle at all.
2. ***Cases with Availability of Correspondent Triangles:*** If increasing the tolerance provides a number of correspondent triangles, the optimal triangle is identified and the ICP algorithm is incorporated using the initial transformation information. Next, performance of the algorithm can be evaluated using the MSE value which can be set to a predefined value depending on the point sets to be matched. The performance can also be evaluated visually. Depending on the performance result, if the MSE value is within a satisfactory limit, the estimated transformation is used as the rigid body transformation to obtain the optimal localization. On the other hand, if the MSE value is not within a satisfactory limit, the measurement

data is further processed by density reduction approach as discussed in step 4 until the optimal localization is achieved.

3. ***Cases with No Available Correspondent Triangle:*** If increasing the tolerance still does not provide any corresponding triangle, density of the measurement point set is reduced according to the next step, step 4.
4. ***Processing Based on Density:*** For this processing based on density, we implement a sequential *density reduction approach* using the ascending density reduced factor $u = u + 1$ in each step of density reduction for the measurement data. As in the preprocessing $u = 1$ has been used, in this processing u starts from 2 and is increased by 1 in every density reduction step.
5. ***Step after Density Reduction*:** After reducing density, the CAD model and the processed measurement data set have to go through step 1 and depending on the availability of the number of correspondence triangles, it either needs to follow either step 2 or step 3.

5.3 Summary of the Algorithm

The proposed initial matching algorithm based on the Delaunay pole sphere, a computational geometric tool invariant under any rigid body transformations, is depicted in Figure 5.4. This algorithm can be summarized by the following steps:

Step 1. The measurement data is preprocessed if it is denser than the CAD model point set, i.e., $\rho_D < \rho_M$. Two point sets obtained from the preprocessed measurement data and the CAD model are considered as the input data for the algorithm.

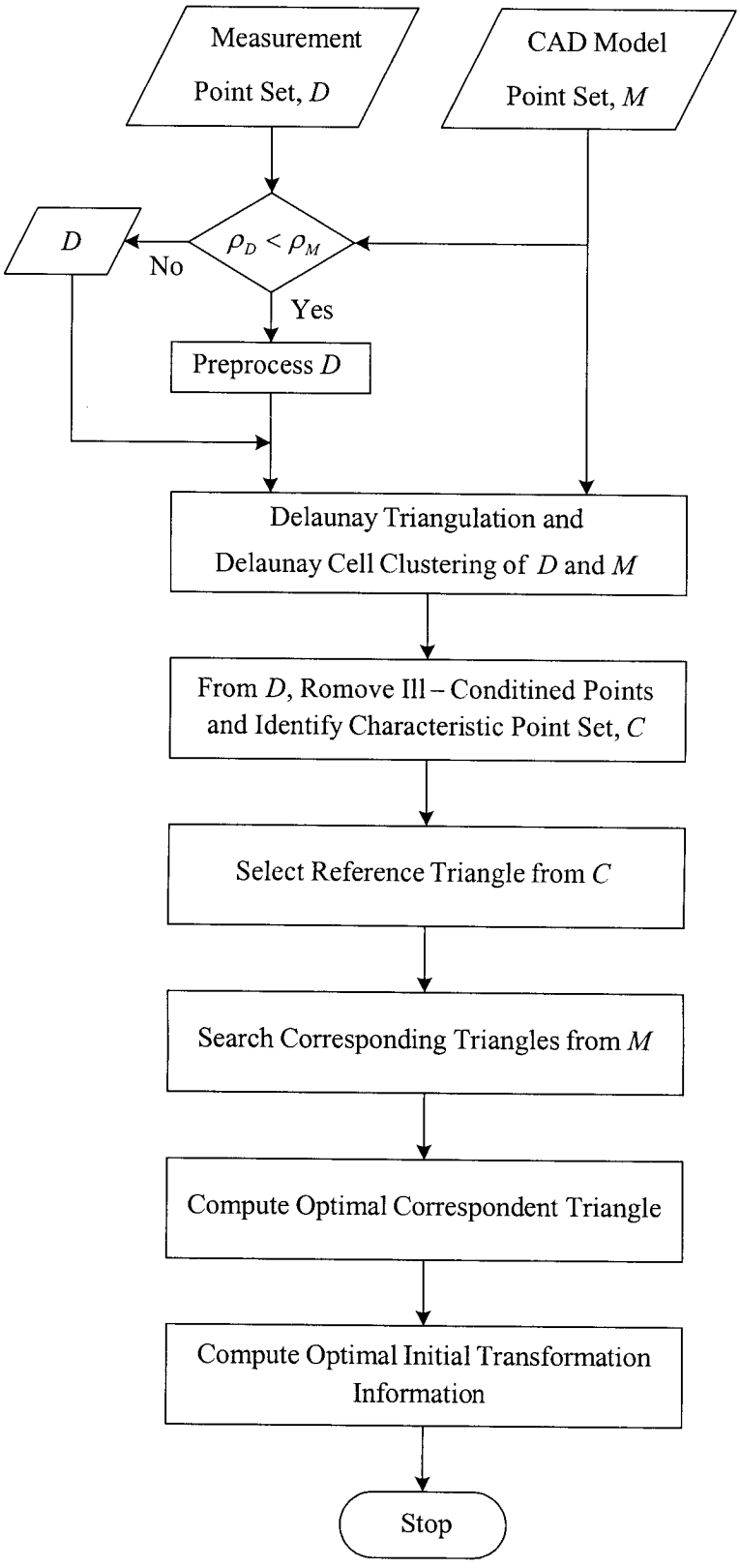

Figure 5.4: Flowchart of the robust initial matching algorithm.

Step 2. Delaunay pole spheres are constructed for each point of the input data by Delaunay triangulation and Delaunay cell clustering of the point sets.

Step 3. Characteristic points are identified and ill-conditioned points are removed from the measurement data set.

Step 4. Three points are selected from those characteristic points to form a reference triangle.

Step 5. Corresponding triangles are searched from the CAD model to correspond the reference triangle and the optimal correspondent triangle is obtained which provides the robust initial transformation information to achieve successful localization.

Chapter 6

Simulation Results

To investigate the effectiveness of the proposed initial matching algorithm, extensive computer simulations have been conducted to test on different objects. All simulation studies are intended to demonstrate the performance of the algorithm on several surfaces having different types of shape complexities. In the context of the simulations environment, it is considered that the objects to be matched are represented by point cloud data. Since surfaces are sampled to form discrete data sets, different distributions of the point cloud data have also been taken into consideration for various tests of this study. Tests are also performed on discrete data sets perturbed by noise to demonstrate the performance of the algorithm to combat the detrimental effects of the disturbance on data.

Surfaces have been generated using their mathematical representations to perform a number of tests since it is easier to investigate the validity of the algorithm using these simulated surfaces of known parameters. On the other hand, in real situation, the data set is obtained in discrete form without any known mathematical representations of the surface. Hence, it necessitates performing some tests using practical data sets to verify this proposed work. In this chapter, the performance evaluation of the proposed algorithm using these two types of test data is presented elaborately.

6.1 Performance Test Using Simulated Data

The major advantage of using simulated data for validating the algorithm is its known mathematical representation with known parameters. These generated surfaces can be handled easily because the data set representing the surfaces does not show any unpredictable behavior. Hence, it is possible to estimate the value of the expected performance index in advance and evaluation can be carried out by comparing with the output obtained from the algorithm. In this way, using simulated data set, it can be proved whether the performance of the proposed algorithm is satisfactory or not. In addition, the level of complexity to be handled by the algorithm can be tested with simulated surfaces with different complexities, i.e., from simple surface to the complex one. These are the reasons for considering the simulated data set for testing the proposed algorithm.

In order to test the proposed algorithm, three surfaces were generated and plotted using NURBS formulation with different parameters in visual C++ platform. The NURBS surface has been chosen over other representations because of its wide acceptability in industry as a standard tool for the representation and design of product geometry. Three surfaces generated with different complexities to evaluate the performance of the proposed approach are depicted in Figure 6.1. These three surfaces are bicubic NURBS surfaces with different surface patch, among which the third surface is the simplest one in complexity, containing less characteristic points than the first two surfaces. The representations of these simulated surfaces in discrete data format are termed as Cloud Data I, Cloud Data II, and Cloud Data III, respectively.

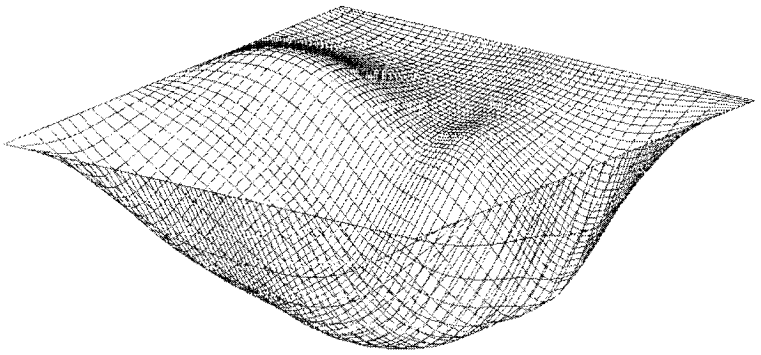

(a) Cloud Data I

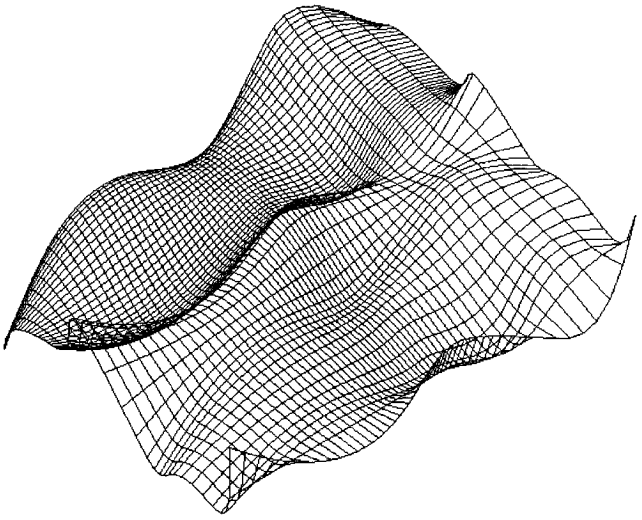

(b) Cloud Data II

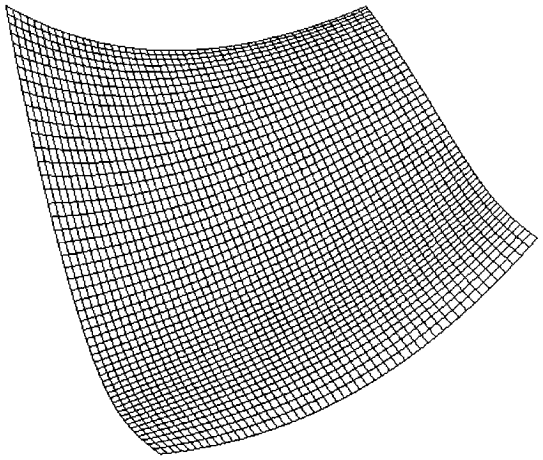

(c) Cloud Data III

Figure 6.1: Typical simulated point cloud data sets examined in the proposed approach.

These three surfaces are generated using the following NURBS formulation [46] with varying parameters:

$$\mathbf{s}(u,v)=\frac{\sum_{i=0}^{n}\sum_{j=0}^{m}w_{i,j}\mathbf{p}_{i,j}B_{i,k}(u)B_{j,l}(v)}{\sum_{i=0}^{n}\sum_{j=0}^{m}w_{i,j}B_{i,k}(u)B_{j,l}(v)},\qquad 0\le u,v\le 1 \tag{6.1}$$

where $w_{i,j}$ represent the weights of the control points, $\mathbf{p}_{i,j}$ form a $(n+1)\times(m+1)$ mesh of control points, $B_{i,k}$ and $B_{j,l}$ are the B-spline basis functions of degree k and l defined over non-uniform and non-periodic knot vectors $\mathbf{u}$ and $\mathbf{v}$ in the u and v directions, respectively,

$$\mathbf{u}=\{\underbrace{u_0,u_1,\ldots,u_k}_{k+1\text{ equal knots}},\underbrace{u_{k+1},u_{k+2},\ldots,u_{r-k-1}}_{r-2k-1\text{ internal knots}},\underbrace{u_{r-k},u_{r-k+1},\ldots,u_r}_{k+1\text{ equal knots}}\} \tag{6.2}$$

$$\mathbf{v}=\{\underbrace{v_0,v_1,\ldots,v_l}_{l+1\text{ equal knots}},\underbrace{u_{l+1},u_{l+2},\ldots,u_{s-l-1}}_{s-2l-1\text{ internal knots}},\underbrace{u_{s-l},u_{s-l+1},\ldots,u_s}_{l+1\text{ equal knots}}\} \tag{6.3}$$

where $r=n+k+1$ and $s=m+l+1$. The basis function in u direction is given by

$$\begin{cases}B_{i,0}(u)=\begin{cases}1, & u_i\le u\le u_{i+1}\\ 0, & \text{otherwise}\end{cases}\\ B_{i,k}(u)=\dfrac{u-u_i}{u_{i+k}-u_i}B_{i,k-1}(u)+\dfrac{u_{i+k+1}-u}{u_{i+k+1}-u_{i+1}}B_{i+1,k-1}(u), \quad k\ge 1\end{cases} \tag{6.4}$$

Each of the first two surfaces is generated with $56\,(7\times 8)$ control points and the third surface is generated with $16\,(4\times 4)$ control points as shown in Appendix B. After generating the surfaces, point clouds are obtained by sampling each simulated surface in a uniform as well as in a random manner.

To initiate the proposed initial matching algorithm, for each surface, two data sets are generated as input to the algorithm by sampling that surface. The first data set is

considered as the CAD model and the other data set is considered as the measurement data. For Cloud Data I, Cloud Data II, and Cloud Data III, the CAD model is generated by sampling respective surface in a uniform manner producing 10,000 (100×100) points and three cases with different measurement data sets are considered for that particular CAD model as shown below.

Case I: measurement data of 2,500 points for Cloud Data I, Cloud Data II, and Cloud Data III is generated as a subset of the respective CAD model data set.

Case II: measurement data of 40,000 (200×200) points for Cloud Data I and Cloud Data II, and measurement data of 22,500 (150×150) points for Cloud Data III, is generated by sampling the respective surface uniformly.

Case III: measurement data of 40,000 (200×200) points for Cloud Data I and Cloud Data II, and measurement data of 22,500 (150×150) points for Cloud Data III, is generated by sampling the respective surface randomly.

After generating each measurement data set, before using as the input to the algorithm, it is transformed to another position. This transformation is achieved using the following 4×4 homogenous transformation matrix:

$$\mathbf{T}=\begin{bmatrix} \cos\alpha\cos\beta & \cos\alpha\sin\beta\sin\gamma-\sin\alpha\cos\gamma & \cos\alpha\sin\beta\cos\gamma+\sin\alpha\sin\gamma & x_t \\ \sin\alpha\cos\beta & \sin\alpha\sin\beta\sin\gamma+\cos\alpha\cos\gamma & \sin\alpha\sin\beta\cos\gamma-\cos\alpha\sin\gamma & y_t \\ -\sin\beta & \cos\beta\sin\gamma & \cos\beta\cos\gamma & z_t \\ 0 & 0 & 0 & 1 \end{bmatrix}$$

where α, β, and γ represent rotation around the x-axis (pitch), rotation around the y-axis (roll), and rotation around the z-axis (yaw), respectively; and x_t, y_t, and z_t represent translation along the x-axis, translation along the y-axis, and translation

along the z-axis, respectively. In our simulation, $\alpha, \beta,$ and γ are chosen to be $145^0, 310^0,$ and 240^0, respectively whereas the values of x_t, y_t, and z_t are taken as 3.0, 7.0, and 4.0, respectively.

Before initiating the correspondence search, the measurement data is preprocessed while needed. For both Case II and Case III, the measurement data set of 40,000 points is preprocessed since it is denser than the CAD model point set of 10,000 points, whereas the measurement data of Case I is not required to be preprocessed. To show the effectiveness of the proposed approach, mean-square error (MSE) between the two point sets under consideration is used as the performance index.

Table 6.1 displays detailed simulation results of the localization algorithm utilizing the proposed initial matching approach where the data sets used for this test are generated from Cloud Data I. The performance of the proposed approach incorporating the ICP algorithm is compared with the direct ICP algorithm proposed in [11]. In this example, the presence of noise has not been considered. In Table 6.2, the detailed simulation results for a similar scenario but with added noise with different levels have been shown. In this case, the measurement data set is sampled uniformly and the noise is considered to be the Gaussian noise added along the normal direction of each point. While dealing with the noisy measurement data, the measurement data sets are processed reducing the density using the proposed density reduction approach until the optimal solution is obtained as discussed in the previous chapter. Similar results are illustrated using Cloud Data II in Table 6.3 without the noise and in Table 6.4 in presence of noise. Table 6.5 and Table 6.6 display elaborate simulation results using data sets generated from Cloud Data III with noise and without noise, respectively.

Table 6.1: Simulation results using Cloud Data I without noise.

Test Case	Input A: Model Point Set		Input B: Measurement Point Set			Preprocessed B		Results Using Initial Matching	Results Using Direct ICP
	Points	Density	Sampling	Points	Density	Points	Density	MSE	MSE
Case I	10,000	0.896	Subset of A	2,500	1.739	-	-	3.527×10^{-9}	32.201
Case II	10,000	0.896	Uniformly	40,000	0.459	10,514	0.799	0.212	26.433
Case III	10,000	0.896	Randomly	40,000	0.467	10,851	0.8109	0.176	24.563

Table 6.2: Simulation results using Cloud Data I with added noise.

Input A: Model Point Set		Input B: Points With Disturbance			Processed B		Results Using Initial Matching	Results Using Direct ICP
Points	Density	Noise Added (%)	Points	Density	Points	Density	MSE	MSE
10,000	0.896	1	40,000	0.458	10,458	0.799	0.206	26.419
10,000	0.896	3	40,000	0.457	3,473	1.400	0.205	26.252
10,000	0.896	5	40,000	0.452	2,547	1.635	0.220	25.983
10,000	0.896	10	40,000	0.454	2,056	1.790	0.209	26.373
10,000	0.896	20	40,000	0.453	1,023	2.789	0.219	26.214
10,000	0.896	50	40,000	0.459	524	3.621	0.209	25.641

Table 6.3: Simulation results using Cloud Data II without noise.

Test Case	Input A: Model Point Set		Input B: Measurement Point Set			Preprocessed B		Results Using Initial Matching	Results Using Direct ICP
	Points	Density	Sampling	Points	Density	Points	Density	MSE	MSE
Case I	10,000	0.995	Subset of A	2,500	1.925	-	-	3.57×10^{-9}	10.681
Case II	10,000	0.995	Uniformly	40,000	0.500	10,136	0.869	0.158	10.306
Case III	10,000	0.995	Randomly	40,000	0.497	9,994	1.007	0.131	10.198

Table 6.4: Simulation results using Cloud Data II with added noise.

Input A: Model Point Set		Input B: Points With Disturbance			Processed B		Results Using Initial Matching	Results Using Direct ICP
Points	Density	Noise Added (%)	Points	Density	Points	Density	MSE	MSE
10,000	0.995	1	40,000	0.503	10,248	0.882	0.164	10.289
10,000	0.995	3	40,000	0.485	9,530	0.886	0.176	10.289
10,000	0.995	5	40,000	0.474	9,111	0.903	0.165	10.302
10,000	0.995	10	40,000	0.462	4315	1.288	0.178	10.264
10,000	0.995	20	40,000	0.449	1,165	2.453	0.164	10.305
10,000	0.995	50	40,000	0.457	843	2.857	0.182	10.264

Table 6.5: Simulation results using Cloud Data III without noise.

Test Case	Input A: Model Point Set		Input B: Measurement Point Set			Preprocessed B		Results Using Initial Matching	Results Using Direct ICP
	Points	Density	Sampling	Points	Density	Points	Density	MSE	MSE
Case I	10,000	0.552	Subset of A	2,500	1.109	-	-	2.07×10^{-9}	39.617
Case II	10,000	0.552	Uniformly	22,500	0.377	10,507	0.547	0.158	39.036
Case III	10,000	0.552	Randomly	22,500	0.375	10,386	0.551	0.037	38.691

Table 6.6: Simulation results using Cloud Data III with added noise.

Input A: Model Point Set		Input B: Points With Disturbance			Processed B		Results Using Initial Matching	Results Using Direct ICP
Points	Density	Noise Added (%)	Points	Density	Points	Density	MSE	MSE
10,000	0.552	1	22,500	0.375	5,177	0.803	0.037	39.027
10,000	0.552	3	22,500	0.451	2,498	1.226	0.037	39.224
10,000	0.552	5	22,500	0.425	1,905	1.195	0.037	39.063
10,000	0.552	10	22,500	0.373	1,026	1.627	0.036	39.127
10,000	0.552	20	22,500	0.358	785	2.194	0.040	39.010
10,000	0.552	50	22,500	0.367	473	2.790	0.044	37.245

It can be seen from all these results that ICP algorithm using initial correspondence knowledge obtained from the proposed initial matching approach renders overwhelming performance compared to the direct ICP algorithm. In terms of performance index and visual observation, it is concluded that ICP algorithm totally fails in some scenarios e.g., for the case of the above mentioned tests, whereas the proposed approach estimates correspondence information robustly providing optimal solution for localization. All the test results displayed in this section dealt with simulated point clouds which are generated from free-form surfaces of different complexities. The performance of the proposed approach considering practical data sets is presented next.

6.2 Performance Test Using Practical Data

Even though the simulation using the theoretical surface with known parameters is an effective way to conduct performance test, the performance of the initial matching algorithm needs to be validated against the practical data. Therefore, tests are also carried out in this study on two practical data sets to show the effectiveness of the proposed algorithm. Between the two practical data sets used in this thesis, the first one is the Stanford Bunny, the most commonly used test model in computer graphics obtained from Stanford Computer Graphics Laboratory [63] in scanned data format. The second one is the Dinosaur Sculpture, one of the sample data sets available from the Cyberware website [64]. This data set is obtained using Cyberware rapid 3D scanner. Figure 6.2 (a) and Figure 6.2 (b) delineate the whole scanned views of the two practical data sets: Stanford Bunny and Dinosaur Sculpture, respectively.

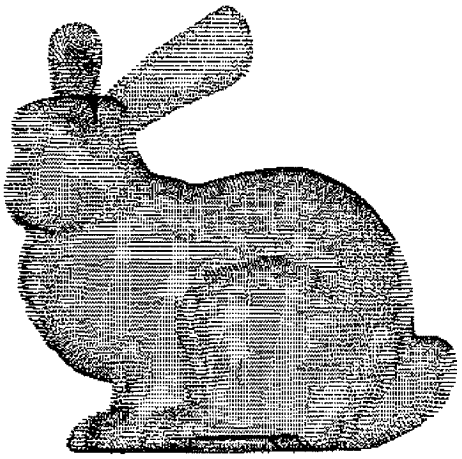

(a) Stanford Bunny

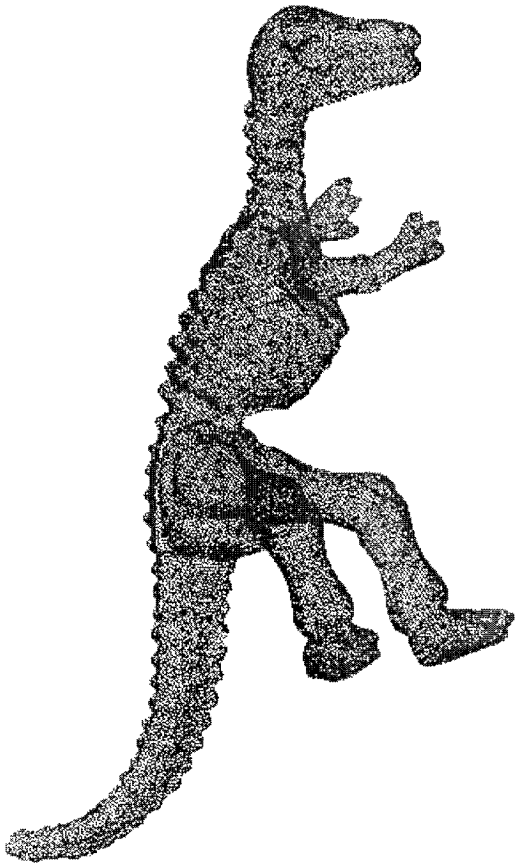

(b) Dinosaur Sculpture

Figure 6.2: Typical practical data sets examined in the proposed approach.

Table 6.7: Simulation results using practical data set.

Test Case	Input A: Model Point Set			Input B: Measurement Point Set			Processed B		Results Using Initial Matching
	Scanned View	Points	Density	Scanned View	Points	Density	Points	Density	MSE
Case I : Stanford Bunny	Whole Bunny	35,947	1.449	One Sided View 1	40,256	0.845	6,851	2.167	0.295
	Whole Bunny	35,947	1.449	One Sided View 2	31,701	0.858	2,781	3.195	0.324
Case II : Dinosaur Sculpture	Half Dinosaur	28,097	0.661	Whole Dinosaur	56,194	0.473	28,796	0.654	0.083

While the test using the Stanford Bunny is conducted, the reconstructed set of the whole Bunny is considered as the CAD model. Two different scanned views have been considered as the two measurement data sets where each view is scanned from single side of the Bunny. Data sets from these two sides are obtained by scanning from two different angles, 0^0 and 270^0, respectively. For testing the proposed approach with the Dinosaur Sculpture, the obtained data set is the scanned view of the whole Dinosaur Sculpture. A subset from this data set is formed such that this subset contains half of the points of the original obtained data and is uniformly distributed over the Dinosaur Sculpture. Hence, the generated data set also represents the geometry of the Dinosaur and is treated in this test as the CAD model data. The whole data set of the Dinosaur Sculpture is considered as the measurement data set to conduct this performance test.

The simulation results using the above two practical data sets are tabulated in Table 6.7. As expected, the proposed approach shows excellent performance to achieve a successful localization for free-form objects. The excellence of using Delaunay pole sphere as an invariant property of any point sets for correspondence search has been proven again.

Chapter 7

Conclusion and Future Directions

This chapter of the thesis concludes with a summary of the proposed approach and avenues for further research work. In product manufacturing, it is a fundamental issue to determine that manufactured object meets the design requirements from which it has been made. The main objective of the research work is to obtain a better inspection system of manufactured products by developing an improved localization technique. This thesis addresses the problem of initial matching of free-form objects and proposes a novel approach to solve it. Only with the availability of very good initial information of the correspondence, a computationally efficient optimal localization can be achieved. This motivated us to focus our attention to develop an algorithm providing optimal initial correspondence information for object matching which has not been studied well so far.

Since any free-form surface can be represented properly by its distinct features, the proposed initial matching algorithm takes resort to the characteristic points of that surface. The proposed method can be applied to the free-form objects and is considered to handle the point (sampled data from parametric surface such as NURBS surface) versus point (discrete measurement data) cases.

7.1 Major Contributions of the Thesis

When no prior knowledge of the transformation or correspondence is available, the localization problem remains a tedious job. To obtain the best transformation for optimal localization, the correspondence search between two surfaces is a key issue. On the other hand, establishing the correspondence between two point sets depends on the availably of the initial correspondence information. T

The major contribution of this thesis can be summarized as follows:

- A robust initial matching approach, which provides the initial transformation information by an optimal correspondence search technique without any prior information of the transformation, is proposed.
- By selecting only three points for correspondence search, in this work, the time and computational complexity of the correspondence search are reduced dramatically.
- Delaunay pole sphere, which is property of a point set and invariant under any rigid body transformation, has been introduced as the specific property for searching correspondence instead of any intrinsic properties of the surface.
- A preprocessing technique applied to the measurement data set based on point density is introduced. Moreover, if the data set is perturbed by any disturbance, a density reduction approach has been implemented to deal with these noisy data.
- Finding the optimal initial correspondence information, the proposed algorithm can be used as the starting point for any standard localization algorithm which depends on the good initial estimate of transformation

7.2 Difficulties of the Proposed Approach

For establishing the correspondence information between point sets, the proposed initial matching approach relies on three characteristic points from the measurement data with specific properties. Hence, this algorithm requires at least three characteristic points from the surface to establish the correspondence information and the surfaces having less than three characteristic points can not be dealt properly with this proposed algorithm.

Because of the unpredictable nature of the data set perturbed by noise, the density reduction approach used to implement the algorithm also depends on the availability of the characteristic points. The density of the point set can not be reduced to combat the detrimental effect of the noise if the reduced data set does not contain at least three characteristic points. Moreover, in case of very noisy measurement data, the performance of the algorithm can not be guaranteed.

7.3 Recommendations for Further Research

Although this thesis had laid an initial matching algorithm for obtaining optimal localization, there are several issues that remain to be explored. We discuss here some important areas where further study could be fruitfully directed, as discussed in the following.

The initial matching algorithm requires two user-defined tolerances for searching initial correspondence of two point sets. These tolerances are very important for the effectiveness of the algorithm. Therefore, the theoretical basis for determination of those

tolerances needs to be established such that the tolerance required for different types of surfaces can be estimated in advance.

For implementing the localization algorithm, the visual checking and the user defined value of the performance index are used for practical data set in the proposed approach. Since the decision of the effectiveness of the method depends on this value of the performance index, a better method for judging the *goodness of fit* can be implemented.

For dealing with the noise affected measurement data set, a density reduction approach is considered in this work. The relationship between the density reduction and the level of noise can be established so that depending on the level of noise (if it is known) of the data set, the density can be reduced accordingly. Moreover, as the behavior of the noisy data set is quite unpredictable, some filtering techniques can be applied to the noisy data to filter out the noise effects before initiating the proposed algorithm.

Taking all aspects into consideration, a suitable automatic localization system can be implemented using the proposed initial matching approach.

Bibliography

[1] N. Amenta, S. Choi, and R. K. Kolluri, "The power crust," in *Proceedings of the 6th ACM Symposium on Solid Modeling and Applications*, Ann Arbor, Michigan, pp. 249-260, June 2001.

[2] N. Amenta, S. Choi, and R. K. Kolluri, "The power crust, unions of balls, and the medial axis transform," Computational Geometry: Theory and Applications, vol. 19(2-3), pp. 127-153, July 2001.

[3] N. Amenta and M. Bern, "Surface reconstruction by Voronoi filtering," *Discrete & Computational Geometry*, vol. 22(4), pp. 481-504, 1999.

[4] N. Amenta, M. Bern, and M. Kamvysselis, "A new Voronoi-based surface reconstruction algorithm," in *Proceedings the 25th SIGGRAPH Annual Conference on Computer Graphics and Interactive Techniques*, vol. 32, pp. 415-421, July 1998.

[5] K. S. Arun, T. S. Huang, and S. D. Blostein, "Least-squares fitting of two 3-D point sets," *IEEE Transactions on Pattern Analysis and Machine Intelligence*, vol. 9(5), pp. 698-700, Sep. 1987.

[6] C. B. Barber, D. P. Dobkin, H. Huhdanpaa, "The Quickhull algorithm for convex hulls," *ACM Transactions on Mathematical Software*, vol. 22(4), pp. 469-83, 1996.

[7] R. Bergevin, D. Laurendeau, and D. Poussart, "Estimating the 3D rigid transformation between two range views of a complex object," in *Proceedings IEEE the 11th IAPR International Conference on Pattern Recognition*, The Hague, The Netherlands, vol. 1, pp. 478-482, 1992.

[8] R. Bergevin, D. Laurendeau and D. Poussart, "Registering range views of multipart objects," *Computer Vision and Image Understanding,* vol. 61(1), pp. 1-16, Jan. 1995.

[9] R. Bergevin, M. Soucy, H. Gagnon, and D. Laurendeau, "Towards a general multi-view registration technique," *IEEE Transactions on Pattern Analysis and Machine Intelligence*, vol. 18(5), pp. 540-547, 1996.

[10] P. J. Besl, "The free-form surface matching problem," in *Machine Vision for Three Dimensional Scenes* (H. Freeman, Ed.). Academic Press, New York, pp. 25-71, 1990.

[11] P. J. Besl and N. D. McKay, "A method for registration of 3-D shapes," *IEEE Transactions on Pattern Analysis and Machine Intelligence*, vol. 14(2), Feb. 1992.

[12] C. Butler, "Investigation into the performance of probes on coordinate measuring machines," *Industrial Metrology*, vol. 2(1), pp 59-70, 1991.

[13] R. J. Campbell and P. J. Flynn, "A survey of free-form object representation and recognition techniques," *Computer Vision and Image Understanding*, vol. 81(2), pp. 166-210, 2001.

[14] C. S. Chua and R. Jarvis, "Point Signatures: a new representation for 3-D object recognition," *International Journal of Computer Vision*, vol. 25(1),

pp. 63- 85, 1997.

[15] Y. Chen and G. Medioni, "Object modeling by registration of multiple range images," *Image and Vision Computing*, vol. 10(3), pp. 145-155, 1992.

[16] T. K. Dey, H. Woo, and W. Zhao. "Approximating medial axis for CAD models," in *Proceedings 8th ACM Symposium on Solid Modeling and Applications*, Seattle, WA, pp. 280-285, June 2003.

[17] C. Dorai and A. K. Jain, "COSMOS - a representation scheme for 3-D free-form objects," *IEEE Transactions on Pattern Analysis and Machine Intelligence*, 19(10), pp. 1115-1130, Oct. 1997.

[18] C. Dorai, G. Wang, A. K. Jain, and C. Mercer, "Registration and integration of multiple object views for 3D model construction," *IEEE Transactions on Pattern Analysis and Machine Intelligence*, vol. 20(1), pp. 83-89, Jan. 1998.

[19] K.-C. Fan and T.-H. Tsai, "Optimal shape error analysis of the matching image for a free-form surface," *Robotics and Computer-Integrated Manufacturing*, vol. 17(3), pp. 215-222, June 2001.

[20] O. D. Faugeras and M. Hebert, "The representation, recognition and locating 3D objects," *International Journal of Robotic Research*, vol. 5(3), pp. 27-52, 1986.

[21] A. Fusiello, U. Castellani, L. Ronchetti, V. Murino, "Model acquisition by registration of multiple acoustic range views," in *Proceedings of Computer Vision–ECCV 2002*, Copenhagen, Denmark, vol. 2351, pp. 805-819, May 2002.

[22] J. P. Heui and J. A. Woo, "Precision inspection system for aircraft parts

having very thin features based on CAD/CAI integration," *International Journal of Advanced Manufacturing Technology*, vol. 12, pp. 442-449, 1996.

[23] B. K. P. Horn, "Extended Gaussian images," *Proceedings of the IEEE,* vol. 72(12), pp. 1671-1686, Dec. 1984.

[24] B. K. P. Horn, "Closed-form solution of absolute orientation using unit quaternions," *Journal of the Optical Society of America*, vol. 4(4), pp. 629-642, April 1987.

[25] B. K. P. Horn, H. M. Hilden, and S. Negahdaripour, "Closed-form solution of absolute orientation using orthonormal matrices," *Journal of the Optical Society of America*, vol. 5(7), pp. 1128-1135, July 1988.

[26] T. S. Huang, S. D. Blostein, and E. A. Margerum, "Least-square estimation of motion parameters from 3-D point correspondences," in *Proceedings IEEE Conference on Computer Vision and Pattern Recognition*, Miami, FL, June 24-26, 1986.

[27] X. Huang and P. Gu, "CAD-model based inspection of sculptured surfaces with datums," *International Journal of Production Research*, vol. 36(5), pp. 1351-1367, May 1998.

[28] X. Huang, P. Gu, and R. Zernicke, "Localization and comparison of two free-form surfaces," *Computer-Aided Design*, vol. 28(12), pp.1017-1022, 1996.

[29] Q. Ge, B. Chen, P. Smith, and C.-H. Menq, "Tolerance specification and comparative analysis for computer-integrated dimensional inspection," *International Journal of Production Research*, vol. 30(9), pp. 2173-2197,

1992.

[30] R. A. Jinkerson, S. L. Abrams, L. Bardis, C. Chryssostomidis, A. Clement, N. M. Patrikaiskis, and F. E. Wolter, "*Inspection and feature extraction of marine propellers*," Journal of Ship Production, vol. 9, pp. 88-106, 1993.

[31] A. E. Johnson and M. Hebert, "Using spin images for efficient object recognition in cluttered 3D scenes," *IEEE Transactions on Pattern Analysis and Machine Intelligence*, 21(5), pp. 433-449, May 1999.

[32] S. B. Kang and K. Ikeuchi, "The complex EGI: a new representation for 3-D pose determination," *IEEE Transactions on Pattern Analysis and Machine Intelligence*, vol. 15(7), pp. 707-721, July 1993.

[33] K. H. Ko, T. Maekawa, and N. M. Patrikalakis, "An algorithm for optimal free-form object matching," *Computer-Aided Design*, vol. 35(10), pp. 913-923, Sept. 2003.

[34] C .C. Kuo and H. T. Yau, "Reconstruction of virtual parts from unorganized scanned data for automated dimensional inspection," *ASME Journal of Computing and Information Science in Engineering*, vol. 3(3), pp. 76-86, 2003.

[35] Y. Li and P. Gu, "Free-form surface inspection techniques - state of the art review," *Computer-Aided Design*, 36(13), pp. 1395-1417, 2004.

[36] Y. Li and P. Gu, "Sculptured surface tolerance verification with design datums," *International Journal of Production Research*, vol. 43(7), pp. 1465-1482, April 2005.

[37] Y. Li and P. Gu, "Inspection of free-form shaped parts," *Robotics and*

Computer-Integrated Manufacturing, vol. 21, pp. 421-430, 2005.

[38] P. Liang and C. H. Taubes, "Orientation-based differential geometric representations for computer vision applications," *IEEE Transactions on Pattern Analysis and Machine Intelligence*, vol. 16(3), pp. 249-258, March 1994.

[39] H. Matsuo and A. Iwata, "3-D object recognition using MEGI model from range data," in *Proceedings 12th International Conference on Pattern Recognition*, Jerusalem, Israel, pp. 843-846, Oct. 1994.

[40] T. Masuda and N. Yokoya, "A robust method for registration and segmentation of multiple range images," *Computer Vision and Image Understanding*, vol. 61(3), pp. 295-307, 1995.

[41] C.-H. Menq, H.-T. Yau, and G.-Y. Lai, "Automated precision measurement of surface profile in CAD-directed inspection," *IEEE Transactions on Robotics and Automation*, vol. 8(2), pp. 268-278, April 1992.

[42] V. S. Nalwa, "Representing oriented piecewise C2 surfaces," *International Journal on Computer Vision*, vol. 3, pp. 131-153, 1989.

[43] I. S. Okatani and K. Deguchi, "A method for fine registration of multiple view range images considering the measurement error properties," *Computer Vision and Image Understanding*, vol. 87(1-3), pp. 66-77, 2002.

[44] D. OuYang and H.-Y. Feng, "Delaunay cell clustering for reconstruction of 2D curves and 3D surfaces," submitted to *IEEE Transactions on Visualization and Computer Graphics*, 2005.

[45] N. M. Patrikalakis and L. Bardis, "Localization of rational B-spline

surfaces," *Engineering with Computers*, vol. 7(4), pp. 237-252, 1991.

[46] L. Piegl, "On NURBS: a survey," *IEEE Computer Graphics and Applications*, vol. 11(1), pp. 55-71, Jan. 1991.

[47] M. Potmesil, "Generating models of solid objects by matching 3D surface segments," in *Proceedings IEEE International Joint Conference on Artificial Intelligence*, Karlsruhe, Germany, pp. 1089-1093, Aug. 1983.

[48] S. Rusinkiewicz and M. Levoy, "Efficient variants of the ICP algorithm," in *Proceedings of the 3rd International Conference on 3D Digital Imaging and Modeling*, Quebec, Canada, pp. 145-152, May 2001.

[49] K. C. Sahoo and C.-H. Menq, "Localization of 3-D objects having complex sculptured surfaces using tactile sensing and surface description," *Journal of Engineering for Industry*, vol. 113, pp. 85-92, Feb. 1991.

[50] P. H. Schönemann, "A generalized solution of the orthogonal procrustes problem," *Psychometrika*, 31(1), pp. 1-10, March 1966.

[51] P. H. Schönemann and R. M. Carroll, "Fitting one matrix to another under choice of a central dilation and a rigid motion," *Psychometrika*, 35(2), pp. 245-255, 1970.

[52] V. Sequeira, K. Ng, E. Wolfart, J. G. M. Goncalves, and D. Hogg, "Automated reconstruction of 3D models from real environments," *ISPRS Journal of Photogrammetry & Remote Sensing*, vol. 54(1), pp. 1-22, 1999.

[53] G. C. Sharp, S. W. Lee, and D. K. Wehe, "ICP registration using invariant features," *IEEE Transactions on Pattern Analysis and Machine Intelligence*, vol. 24(1), Jan. 2002.

[54] F. Stein and G. Medioni "Structural indexing: efficient 3-D object recognition," *IEEE Transactions on Pattern Analysis and Machine Intelligence*, vol. 14(2), pp. 125-145, Feb. 1992.

[55] S. Umeyama, "Least-squares estimation of transformation parameters between two point patterns," *IEEE Transaction on Pattern Analysis and Machine Intelligence*, vol. 13(4), pp. 376-380, April 1991.

[56] F. S. Voronoi, "Diagrams and Delaunay triangulations," in *Computing in Euclidean Geometry*, 2nd Edition, Lecture Notes Series on Computing, World Scientific, vol. 4, pp. 225-65, 1995.

[57] M. W. Walker, L. Shao, and R. A. Volz, "Estimating 3-D location parameters using dual number quaternions," *CVGIP: Image Understanding*, vol. 54(3), pp. 358-367, Nov. 1991.

[58] J. Williams and M. Bennamoun, "Simultaneous registration of multiple corresponding point sets," *Computer Vision and Image Understanding*, 81(1), pp. 117-142, Jan. 2001.

[59] S. M. Yamany, A. A. Fraag, and A. El-Bialy, "Free-form surface registration and object recognition using surface signatures," in *Proceedings IEEE International Conference on Computer Vision*, Kerkyra, Grece, 1999.

[60] Z. Zhang, "Iterative point matching for registration of free-form curves and surfaces," *International Journal of Computer Vision*, vol. 13(2), pp. 119-152, 1994.

[61] D. Zhang and M. Hebert, "Harmonic maps and their applications in surface matching," in *Proceedings IEEE Conference in Computer Vision and*

Pattern Recognition, Colorado, vol. 2, pp. 524-530, June 1999.

[62] http://www.cgal.org/

[63] http://www-graphics.stanford.edu/

[64] http://www.cyberware.com/samples/

Appendix A

Calculation of Circum-Sphere

The equation for the circum-circle of a tetrahedron with polygon vertices (x_i, y_i, z_i) for $i = 1, 2, \ldots, 4$ is give by the following form

$$\begin{vmatrix} x^2+y^2+z^2 & x & y & z & 1 \\ x_1^2+y_1^2+z_1^2 & x_1 & y_1 & z_1 & 1 \\ x_2^2+y_2^2+z_2^2 & x_2 & y_2 & z_2 & 1 \\ x_3^2+y_3^2+z_3^2 & x_3 & y_3 & z_3 & 1 \\ x_4^2+y_4^2+z_4^2 & x_4 & y_4 & z_4 & 1 \end{vmatrix} = 0 \qquad \text{(A.1)}$$

Expanding the determinant of (A.1) we get

$$a(x^2+y^2+z^2)+(b_x x+b_y y+b_z z)+c=0 \qquad \text{(A.2)}$$

where

$$a = \begin{vmatrix} x_1 & y_1 & z_1 & 1 \\ x_2 & y_2 & z_2 & 1 \\ x_3 & y_3 & z_3 & 1 \\ x_4 & y_4 & z_4 & 1 \end{vmatrix}, \qquad \text{(A.3)}$$

b_x is the determinant obtained from the matrix

$$D = \begin{bmatrix} x_1^2 + y_1^2 + z_1^2 & x_1 & y_1 & z_1 & 1 \\ x_2^2 + y_2^2 + z_2^2 & x_2 & y_2 & z_2 & 1 \\ x_3^2 + y_3^2 + z_3^2 & x_3 & y_3 & z_3 & 1 \\ x_4^2 + y_4^2 + z_4^2 & x_4 & y_4 & z_4 & 1 \end{bmatrix} \tag{A.4}$$

by discarding the x_i column (and taking a plus sign), b_y is the determinant obtained from the matrix D by discarding the y_i column (and taking the minus sign), b_z is the determinant obtained from the matrix D by discarding the z_i column (and taking the plus sign) given by

$$b_x = + \begin{vmatrix} x_1^2 + y_1^2 + z_1^2 & y_1 & z_1 & 1 \\ x_2^2 + y_2^2 + z_2^2 & y_2 & z_2 & 1 \\ x_3^2 + y_3^2 + z_3^2 & y_3 & z_3 & 1 \\ x_4^2 + y_4^2 + z_4^2 & y_4 & z_4 & 1 \end{vmatrix} \tag{A.5}$$

$$b_y = - \begin{vmatrix} x_1^2 + y_1^2 + z_1^2 & x_1 & z_1 & 1 \\ x_2^2 + y_2^2 + z_2^2 & x_2 & z_2 & 1 \\ x_3^2 + y_3^2 + z_3^2 & x_3 & z_3 & 1 \\ x_4^2 + y_4^2 + z_4^2 & x_4 & z_4 & 1 \end{vmatrix} \tag{A.6}$$

$$b_z = + \begin{vmatrix} x_1^2 + y_1^2 + z_1^2 & x_1 & y_1 & 1 \\ x_2^2 + y_2^2 + z_2^2 & x_2 & y_2 & 1 \\ x_3^2 + y_3^2 + z_3^2 & x_3 & y_3 & 1 \\ x_4^2 + y_4^2 + z_4^2 & x_4 & y_4 & 1 \end{vmatrix} \tag{A.7}$$

and c is given by

$$c = - \begin{vmatrix} x_1^2 + y_1^2 + z_1^2 & x_1 & y_1 & z_1 \\ x_2^2 + y_2^2 + z_2^2 & x_2 & y_2 & z_2 \\ x_3^2 + y_3^2 + z_3^2 & x_3 & y_3 & z_3 \\ x_4^2 + y_4^2 + z_4^2 & x_4 & y_4 & z_4 \end{vmatrix}. \tag{A.8}$$

Completing the square gives

$$a\left(x+\frac{b_x}{2a}\right)^2+a\left(y+\frac{b_y}{2a}\right)^2+a\left(z+\frac{b_z}{2a}\right)^2-\frac{b_x^2+b_y^2+b_z^2}{4a}+c=0 \tag{A.9}$$

which is a circum-sphere of the form

$$(x-x_0)^2+(y-y_0)^2+(y-y_0)^2=r^2 \tag{A.10}$$

with circum-center

$$x_0=\frac{b_x}{2a} \tag{A.11}$$

$$y_0=\frac{b_y}{2a} \tag{A.12}$$

$$z_0=\frac{b_z}{2a} \tag{A.13}$$

and circum-radius

$$r=\frac{\sqrt{b_x^2+b_y^2+b_z^2-4ac}}{2a}. \tag{A.14}$$

Appendix B

Control Points of Simulated Surfaces

We simulate three test surfaces with their NURBS surface representations as explained in Chapter 6. Each of the first two surfaces is generated with 56 (7×8) control points and the third surface is generated with 16 (4×4) control points as shown below.

B.1 Control Points for NURBS Surface I (Cloud Data I)

[P] =

$$\begin{bmatrix}
(0,00,10) & (10,00,10) & (20,00,10) & (30,00,10) & (40,00,10) & (40,00,10) & (60,00,10) & (70,00,10) \\
(0,10,10) & (10,10,00) & (20,10,-10) & (30,10,-10) & (40,10,-20) & (50,10,-10) & (60,10,10) & (70,10,10) \\
(0,20,10) & (10,20,-10) & (20,20,-20) & (30,20,-20) & (40,20,-10) & (50,20,00) & (60,20,00) & (70,20,10) \\
(0,30,10) & (10,30,-10) & (20,30,-20) & (30,30,-10) & (40,30,00) & (50,30,10) & (60,30,00) & (70,30,10) \\
(0,40,10) & (10,40,-10) & (20,40,00) & (30,40,-10) & (40,40,00) & (50,40,00) & (60,40,10) & (70,40,10) \\
(0,50,10) & (10,50,-10) & (20,50,00) & (30,50,10) & (40,50,20) & (50,50,20) & (60,50,-10) & (70,50,10) \\
(0,70,10) & (10,70,10) & (20,70,10) & (30,70,10) & (40,70,10) & (50,70,10) & (60,70,10) & (70,70,10)
\end{bmatrix}$$

B.2 Control Points for NURBS Surface II (Cloud Data II)

[**P**] =

$$\begin{bmatrix} (00,00,10) & (10,00,-10) & (20,00,10) & (30,00,-10) & (40,00,10) & (50,00,-10) & (60,00,10) & (70,00,-10) \\ (00,10,-10) & (10,10,10) & (20,10,-10) & (30,10,10) & (40,10,-10) & (50,10,10) & (60,10,-10) & (70,10,10) \\ (00,20,00) & (10,20,-20) & (20,20,00) & (30,20,00) & (40,20,00) & (50,20,-20) & (60,20,00) & (70,20,00) \\ (00,30,10) & (10,30,-10) & (20,30,10) & (30,30,-10) & (40,30,10) & (50,30,-10) & (60,30,00) & (70,30,-10) \\ (00,40,10) & (10,40,-10) & (20,40,00) & (30,40,-10) & (40,40,10) & (50,40,-10) & (60,40,10) & (70,40,-10) \\ (00,50,-10) & (10,50,10) & (20,50,-10) & (30,50,10) & (40,50,-10) & (50,60,-20) & (60,50,-10) & (70,60,10) \\ (00,70,20) & (10,70,-10) & (20,70,10) & (30,70,-20) & (40,70,20) & (50,70,-10) & (60,70,10) & (70,70,-20) \end{bmatrix}$$

B.3 Control Points for NURBS Surface III (Cloud Data III)

[**P**] =

$$\begin{bmatrix} (00,00,50) & (10,00,10) & (20,00,10) & (30,00,-20) \\ (00,10,00) & (10,10,-20) & (20,10,10) & (30,10,-20) \\ (00,20,00) & (10,20,-10) & (20,20,-20) & (30,20,00) \\ (00,30,20) & (10,30,-20) & (20,30,-10) & (30,30,60) \end{bmatrix}$$

Curriculum Vita

Name	Nimun A. Jahangir
Post Secondary Education	
2005	Master of Engineering Science (M.E.Sc.) The University of Western Ontario London, Ontario, Canada
2001	Bachelor of Science in Engineering Bangladesh Institute of Technology Chittagong, Bangladesh
Scholarship/Awards	
1996-2001	Government Scholarship for Undergraduate Study Ministry of Education Bangladesh
1997-2001	University Merit Scholarship Bangladesh Institute of Technology Chittagong, Bangladesh
Related Experience	
2003-2005	Research Assistant The University of Western Ontario

2003-2005	Teaching Assistant The University of Western Ontario

Professional Experience

2001-2002	Design Engineer Sanmar Software, Sanmar Group Bangladesh
2001	Trainee Work Study Executive Chittagong Export Processing Zone Chittagong, Bangladesh.